NEXT-MOL: 3D DIFFUSION MEETS 1D LANGUAGE MODELING FOR 3D MOLECULE GENERATION

Anonymous authors
Paper under double-blind review

ABSTRACT

3D molecule generation is crucial for drug discovery and material design. While prior efforts focus on 3D diffusion models for their benefits in modeling continuous 3D conformers, they overlook the advantages of 1D SELFIES-based Language Models (LMs), which are able to generate 100% valid molecules and leverage the billion-scale 1D molecule datasets. To combine these advantages for 3D molecule generation, we propose a foundation model – NEXT-Mol: 3D Diffusion Meets 1D Language Modeling for 3D Molecule Generation. NEXT-Mol uses an extensively pretrained molecule LM for 1D molecule generation, and subsequently predicts the generated molecule's 3D conformers with a 3D diffusion model. We enhance NEXT-Mol's performance by scaling up the LM's model size, refining the diffusion neural architecture, and applying 1D to 3D transfer learning. Notably, we demonstrate that incorporating 1D representations from our molecule LM improves the 3D diffusion model's conformer prediction by 1.3% coverage-recall on GEOM-DRUGS. Given these improvements, NEXT-Mol achieves leading performances in *de novo* 3D molecule generation, 3D conformer prediction, and conditional 3D molecule generation, demonstrating its effectiveness and versatility as a foundation model in the field. Our codes and pretrained checkpoints are available at https://anonymous.4open.science/r/NEXT-Mol.

1 INTRODUCTION

Molecule discovery is crucial for designing new drugs and materials. To efficiently navigate the astronomical chemical space of molecules, generative deep learning methods have been extensively explored. While promising progress has been made in generating 2D molecular graphs (Jin et al., 2018; Vignac et al., 2023a), recent research has shifted toward 3D molecule generation due to its broader application scope. For example, understanding the 3D molecular geometry is crucial for structure-based drug design (Zhang et al., 2023), prediction of molecular quantum chemical properties (Zhou et al., 2023), and molecular dynamic simulation (Hansson et al., 2002).

3D molecule generation aims to predict 3D molecular conformers along with their 2D graphs (Hoogeboom et al., 2022). These generated 3D molecules are typically evaluated based on their molecular validity and stability, ensuring adherence to the chemical valency rules. Recent advancements in 3D diffusion models (Vignac et al., 2023b; Hua et al., 2023; Huang et al., 2024) have improved these metrics by better modeling continuous 3D conformers, yet they still occasionally generate invalid molecules. This hinders learning other molecular attributes beyond validity, like functional groups, which are defined only for valid structures. For improvement, we draw inspiration from 1D molecule generation (Fang et al., 2024; Polykovskiy et al., 2020) studies, which reliably ensure 100% validity. By representing 2D molecular graphs as linear strings of SELFIES (Krenn et al., 2020), these approaches typically leverage 1D language models (LMs) for 2D molecule generation. Due to SELFIES' inherent robustness, the generated molecules are guaranteed to be 100% valid. Inspired by these studies, a natural solution for improving 3D molecule generation is to incorporate a 1D SELFIES-based LM into a 3D diffusion model (Jing et al., 2022), thus leveraging the chemical validity of 1D representations while improving 3D conformer prediction. To our best knowledge, few prior research has thoroughly explored this incorporation for 3D molecule generation.

To bridge the research gap above, we explore a two-step solution for 3D molecule generation: initially generating a 1D molecule (a subset of a 3D molecule) using an LM and subsequently predict-

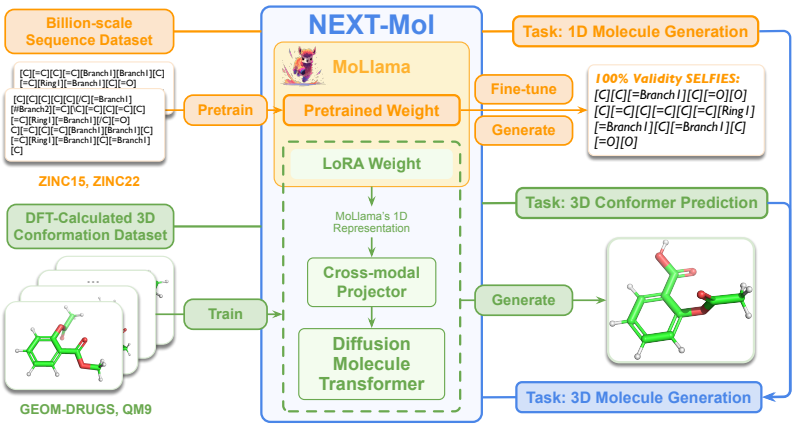

Figure 1: Overview of our NEXT-Mol foundation model for 3D molecule generation. NEXT-Mol consists of three key components: (1) MoLlama, a large LM for generating 1D molecule sequences; (2) DMT, a diffusion model to predict 3D conformers from the 1D sequences; and (3) NEXT-Mol leverages transfer learning to enhance DMT's 3D prediction with MoLlama's 1D representations.

ing its 3D conformer with a diffusion model. Here we focus on three key strategies — scaling up 1D molecular LMs, refining the architecture of 3D diffusion models, and utilizing transfer learning between 1D and 3D modeling — to resolve the following three challenges faced by prior studies:

- **The Development of An Effective 1D Molecular LM.** This can be done by training an autoregressive transformer LM (Vaswani et al., 2017) on a large SELFIES corpus. However, existing studies have the following limitations: some use non-autoregressive pretraining, rendering them unsuitable for *de novo* generation (Fang et al., 2024; Irwin et al., 2022; Born & Manica, 2023; Yüksel et al., 2023); some do not have 100% validity (Bagal et al., 2021); and others are constrained by small model sizes and employ non-transformer architectures, limiting their scalability (Polykovskiy et al., 2020; Eckmann et al., 2022; Arús-Pous et al., 2019; Jin et al., 2018).
- **The Design of A Powerful 3D Diffusion Model.** This is to accurately generate the 3D conformers for the 1D molecules generated by the 1D molecular LM in the earlier step. However, existing works either exhibit limited performance (Jing et al., 2022; Corso et al., 2024; Xu et al., 2022; Ganea et al., 2021) or are not open-source (Wang et al., 2024), preventing their adaptation for future research. Moreover, the neural architecture in the prominent MCF study (Wang et al., 2024) can be improved by leveraging the full information of 2D molecular graphs.
- **Transfer Learning between 1D Molecule Sequences and 3D Conformers.** It has the potential to offer a significant improvement to 3D conformer prediction, given the greater availability of 1D sequences compared to high-accuracy 3D conformers, which are typically derived by expensive DFT calculations. For example, the ZINC22 (Tingle et al., 2023) database now includes over 54.9 billion 1D molecule sequences and the GEOM (Axelrod & Gomez-Bombarelli, 2022) database holds only 37 million 3D conformers. Although this 1D to 3D transfer learning has been successfully applied to 3D protein structure prediction (Lin et al., 2023; Wu et al., 2022), similar methods remain mostly unexplored for small molecules, indicating a significant research opportunity.

To address the challenges above, we propose a foundation model – **NEXT-Mol**: 3D Diffusion Meets 1D Language Modeling for 3D Molecule Generation, as illustrated in Figure 1. NEXT-Mol consists of three key components: (1) To achieve effective autoregressive 1D molecule generation, we pretrain a Molecular Llama LM (**MoLlama**) (Touvron et al., 2023; Zhang et al., 2024) on a large collection of 1.8B SELFIES sequences. This extensive pretraining empowers MoLlama to effectively capture the desired 1D/2D molecular patterns (*e.g.,* scaffolds and fragments) in downstream datasets, laying a strong foundation for the subsequent 3D conformer prediction. (2) To achieve high-accuracy 3D conformer prediction, we introduce a novel diffusion model – Diffusion Molecular Transformer (**DMT**). DMT combines the power of a scalable neural architecture (Wang et al., 2024) and retains the full information of 2D molecular graphs by incorporating the Relational Multi-Head Self-Attention (Huang et al., 2024) that extends the standard self-attention by incorporating pair information describing atomic interactions. Our results demonstrate that DMT could achieve leading performance for 3D conformer prediction, accurately revealing 3D structures of MoLlama-generated

1D molecules with improved performance across six 3D-metrics of stability and geometric similarity. (3) We demonstrate that transfer learning between 1D molecular sequences and 3D conformers significantly improves the conformer prediction performance. Specifically, we leverage MoLlama's 1D representations to enhance DMT's 3D prediction. We bridge the gap between MoLlama and DMT through a cross-modal projector and the corresponding training strategy (Liu et al., 2024).

Collectively, our NEXT-Mol foundation model is a versatile multi-task learner, and demonstrates leading performances for *de novo* 3D molecule generation, 3D conformer prediction, and conditional 3D molecule generation on the GEOM-DRUGS, GEOM-QM9 (Axelrod & Gomez-Bombarelli, 2022) and QM9-2014 (Ramakrishnan et al., 2014) datasets. The strong performance highlights NEXT-Mol's effectiveness and its potential impact as a foundation model in the field. We further present extensive ablation studies to demonstrate the significance of each component of NEXT-Mol.

2 Related Works

A complete molecule includes atoms, bonds, and the 3D coordinates of atoms (*i.e.,* 3D conformer). However, due to the expensive computation for obtaining high-accuracy 3D conformers (Axelrod & Gomez-Bombarelli, 2022), many studies focus on generating atoms and bonds without 3D conformers, representing molecules as 1D sequences or 2D graphs. Here we begin by reviewing 1D and 2D molecule generation, then discuss 3D molecule generation and 3D conformer prediction.

1D and 2D Molecule Generation aims to generate the atoms and bonds of a molecule. 1D generation works are mostly based on LMs. However, they usually apply non-autoregressive pretraining such as span-prediction (Irwin et al., 2022; Fang et al., 2024; Born & Manica, 2023), making them unsuitable for *de novo* generation. Other works use non-transformer architecture (Arús-Pous et al., 2019; Polykovskiy et al., 2020; Flam-Shepherd et al., 2022; Gómez-Bombarelli et al., 2018; Eckmann et al., 2022; Popova et al., 2018), which are unsuitable for scale-up (Vaswani et al., 2017). 2D molecule generation works typically decompose molecular graphs as functional fragments (or atoms), and train models to recurrently generate or edit these fragments (Jin et al., 2018; Xie et al., 2021; Luo et al., 2021; Shi et al., 2020; Sun et al., 2022; Liu et al., 2018; You et al., 2018; Popova et al., 2019; Jin et al., 2019). However, due to their non-transformer architectures and domain-specialized training methods, these 2D generation models also face challenges with scalability and transfer learning. We refer readers to (Du et al., 2022) for a comprehensive survey in this area.

3D Molecule Generation is dominated by diffusion models (Hoogeboom et al., 2022; Bao et al., 2023; Huang et al., 2023a; 2024; 2023b; Vignac et al., 2023b; Hua et al., 2023). While autoregressive methods have been explored (Gebauer et al., 2019; 2022; Luo & Ji, 2022; Simm et al., 2020), they underperform diffusion models, potentially due to their inability to model bonds and the error accumulation when autoregressively generating 3D coordinates. Diffusion models typically employ 3D equivariant neural networks (Satorras et al., 2021) to denoise the variables of atoms, bonds, and 3D coordinates within a single diffusion process. However, they predict molecules without validity constraints and are limited by insufficient 3D data. To address these issues, we aim to integrate the two advantages of 1D SELFIES sequences – 100% validity and the more abundant dataset (Sterling & Irwin, 2015; Tingle et al., 2023) – into 3D molecule generation for improvement.

3D Conformer Prediction is to predict the 3D conformer given the atoms and bonds of a molecule (Xu et al., 2022; Ganea et al., 2021; Zhou et al., 2023; Jing et al., 2022; Corso et al., 2024). The current state-of-the-art approach scales up a diffusion model using a general-purpose transformer architecture (Wang et al., 2024), but it overlooks the chemical bond information and uses a lossy representation of molecular structures. We address these issues by introducing the DMT architecture that maintains scalability and retains the full information of 2D molecular graphs.

3 3D Diffusion Meets 1D LM for 3D Molecule Generation

NEXT-Mol for 3D Molecule Generation. NEXT-Mol is a foundation model that generates 3D molecules with a two-step method: initially generating the 1D molecule sequence using the MoLlama LM and subsequently predicting its 3D conformer using the DMT diffusion model. Here we begin by introducing the MoLlama LM for 1D molecule generation and then proceed to the DMT diffusion model. Finally, we detail the transfer learning method to incorporate MoLlama's 1D representation to enhance DMT's 3D conformer prediction. Appendix C includes implementation details.

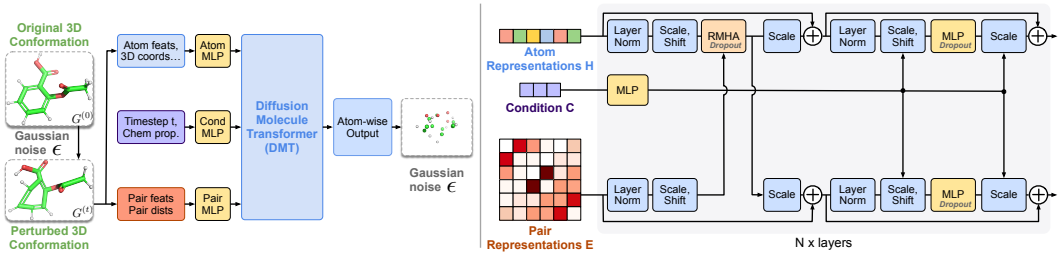

(a) DMT's diffusion process. **(b)** Detailed view of each DMT layer.

Figure 2: Overview of DMT's neural architecture. **(a)** DMT is a diffusion model learning to denoise random Gaussian perturbations $\boldsymbol{\epsilon}$ applied on the 3D coordinates of atoms. **(b)** DMT relies on the RMHA module to iteratively update atom representations $\mathbf{H}$ and pair representations $\mathbf{E}$.

3.1 1D Molecule Generation with Molecular Llama LM

Data Preparation. Following (Irwin et al., 2022), we collect 1.8 billion molecules from the ZINC-15 database (Sterling & Irwin, 2015), significantly more than the 100 million molecules used in previous studies (Irwin et al., 2022; Fang et al., 2024). We preprocess the molecules to transform them into SELFIES and perform data filtering to avoid overlap with the downstream datasets. The resulting dataset contains 90 billion SELFIES tokens.

Pretraining MoLlama. Our MoLlama is a 960M parameter LM with the popular decoder-only Llama-2 (Touvron et al., 2023) architecture. We pretrain it from scratch for 1D molecule generation with the next-token prediction objective. The pretraining takes 555K global steps, processing 145 billion tokens, which amounts to approximately 1.6 passes through the pretraining dataset.

Randomized SELFIES Augmentation. We use randomized SELFIES as data augmentations during fine-tuning MoLlama for 1D molecule generation. A molecule can have multiple valid SELFIES, because they are generated by traversing the 2D molecular graph in different orders. Randomized SELFIES are generated by traversing in random orders. This approach improves sample diversity and mitigates overfitting compared to using the canonical traversal order (Arús-Pous et al., 2019). The intuition is that the atoms in a molecule are inherently unordered, therefore an ideal LM should generate different orderings of the same molecule with equal likelihood.

3.2 3D Conformer Prediction with Diffusion Molecular Transformer

Here we elaborate on the three key components of our proposed DMT: (1) the diffusion process governing the training and inference; (2) the neural architecture; and (3) the rotation augmentation.

Diffusion Process. A molecule $G = (\mathbf{x}, \mathbf{h}, \mathbf{e})$ is represented by its 3D coordinates $\mathbf{x} \in \mathbb{R}^{N\times 3}$, atom features $\mathbf{h} \in \mathbb{R}^{N\times d_1}$ (*e.g.,* atom types), and pair features $\mathbf{e} \in \mathbb{R}^{N\times N\times d_2}$ (*e.g.,* chemical bonds), where N is the number of atoms and d_1 and d_2 are the feature dimensions. For 3D conformer prediction, we use a continuous-time diffusion model (Kingma et al., 2021) that denoises a molecule's 3D coordinates $\mathbf{x}$ based on its atom and pair features. As Figure 2a shows, in the forward diffusion process, noises are gradually applied to the original 3D coordinates $\mathbf{x}^{(0)} = \mathbf{x}$ such that $q(\mathbf{x}^{(t)}|\mathbf{x}^{(0)}) = \mathcal{N}(\mathbf{x}^{(t)}; \sqrt{\bar{\alpha}^{(t)}}\mathbf{x}^{(0)}, (1-\bar{\alpha}^{(t)})\mathbf{I})$, where $t \in (0, 1]$ is the diffusion's time-step, and $\bar{\alpha}^{(t)}$ is a hyperparameter controlling the noise scale at the t step. Based on the reparameterization trick (Ho et al., 2020), we can sample $\mathbf{x}^{(t)} = \sqrt{\bar{\alpha}^{(t)}}\mathbf{x}^{(0)} + \sqrt{1-\bar{\alpha}^{(t)}}\boldsymbol{\epsilon}^{(t)}$, where $\boldsymbol{\epsilon}^{(t)} \sim \mathcal{N}(\mathbf{0}, \mathbf{I})$. Given the perturbed coordinates $\mathbf{x}^{(t)}$, DMT is trained to predict the noise $\boldsymbol{\epsilon}^{(t)}$ by minimizing the MSE loss $\mathcal{L} = \|\boldsymbol{\epsilon}^{(t)} - \text{DMT}(G^{(t)}, t)\|_2^2$, where $G^{(t)} = (\mathbf{x}^{(t)}, \mathbf{h}, \mathbf{e})$. After training, DMT can be employed for 3D conformer prediction through ancestral sampling (Ho et al., 2020).

Neural Architecture. As Figure 2b illustrates, DMT adopts Relational Multi-Head Self-Attention (**RMHA**) (Huang et al., 2024) and adaptive layernorm (adaLN) (Perez et al., 2018; Peebles & Xie, 2023). adaLN replaces the learnable scale and shift parameters in standard layernorm (Ba, 2016) with adaptive ones that are generated from the condition embedding $\mathbf{C}$, which combines the time-step and optionally a desired chemical property. For simplicity, we omit adaLNs in discussion below.

The philosophy behind DMT's neural architecture generally follows the "bitter lesson" recently revealed by MCF (Wang et al., 2024) that large scalable models outperform domain-specific inductive biases. Notably, MCF shows that it is unnecessary to have an architecture of built-in 3D equivari-

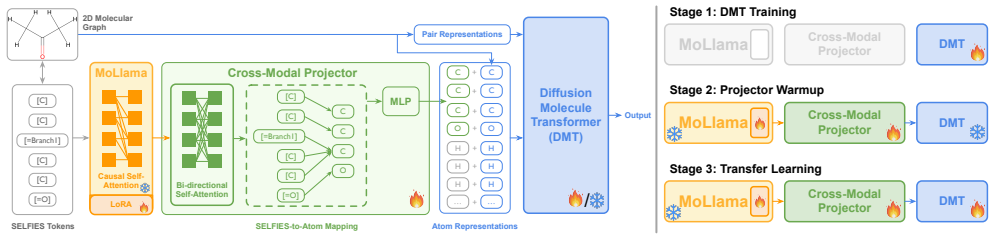

(a) Cross-modal projector bridges MoLlama and DMT. **(b)** Three training stages for 1D to 3D transfer learning.

Figure 3: Transfer learning between MoLlama's 1D representations and DMT's 3D prediction. **(a)** A cross-modal projector bridges the gap between MoLlama and DMT. Grey H atoms have no corresponding SELFIES tokens, and are replaced by a learnable token. **(b)** Transfer learning's three training stages. Snowflake ❄ denotes frozen parameters while flame 🔥 denotes trainable ones.

ance for conformer prediction. However, MCF is limited to employing a lossy representation of 2D molecular structures and overlooks bond information, by relying on the top-k eigenvectors of the graph Laplacian (Maskey et al., 2022) to represent 2D molecular graphs. To address this issue, DMT retains the full information of 2D molecular graphs in its atom representation $\mathbf{H} \in \mathbb{R}^{N\times d}$ and pair representation $\mathbf{E} \in \mathbb{R}^{N\times N\times d}$, and then applies RMHA to learn and distinguish the 2D graph structures. Specifically, the atom representations $\mathbf{H}$ are initialized by concatenating the atom features $\mathbf{h}$ and the perturbed 3D coordinates $\mathbf{x}^{(t)}$, the pair representations $\mathbf{E}$ are initialized by concatenating the pair features $\mathbf{e}$ and the distances between each atom pair. $\mathbf{H}$ and $\mathbf{E}$ are then iteratively refined by RMHA. The single-head RMHA is defined below with the multi-head version in Appendix C.2:

$$[\mathbf{Q};\mathbf{K};\mathbf{V}] = [\mathbf{W}_q;\mathbf{W}_k;\mathbf{W}_v]\mathbf{H}^\top, \quad (1) \qquad [\mathbf{Q}^E;\mathbf{V}^E] = \tanh([\mathbf{W}_{eq};\mathbf{W}_{ev}]\mathbf{E}^\top), \quad (2)$$

$$a_{i,j} = \mathrm{softmax}_j\left(\frac{(\mathbf{Q}^E_{i,j}\odot\mathbf{Q}_i)\mathbf{K}_j^\top}{\sqrt{d}}\right), \quad (3) \qquad \mathbf{O}_i = \sum_{j=1}^{N} a_{i,j}(\mathbf{V}^E_{i,j}\odot\mathbf{V}_j), \quad (4)$$

where $\odot$ denotes element-wise product; $\mathrm{softmax}_j$ denotes softmax along the j dimension; linear projectors $\mathbf{W}_q$, $\mathbf{W}_k$, and $\mathbf{W}_v$ generate queries, keys, and values for atom representations, $\mathbf{W}_{eq}$ and $\mathbf{W}_{ev}$ generate queries and values for pair representations; $\mathbf{O}_i$ is RMHA's output for the i-th atom; and $\mathbf{Q}^E_{i,j}, \mathbf{V}^E_{i,j} \in \mathbb{R}^d$ are the query and value for the atom pair representation (i,j).

RMHA uses the pair-level query $\mathbf{Q}^E_{ij}$ and key $\mathbf{V}^E_{ij}$ of $\mathbf{E}$ to modify the nodel-level query $\mathbf{Q}_i$ and value $\mathbf{V}_j$ through element-wise multiplication ($\odot$), enabling RMHA to fully incorporate pair representations. Specifically, the pair $\mathbf{E}$ affects attention scores via $(\mathbf{Q}^E_{ij}\odot\mathbf{Q}_i)\mathbf{K}_j^\top$, and affects the aggregated attention values via $\mathbf{V}^E_{ij}\odot\mathbf{V}_j$. In this way, the output $\mathbf{O}$ is adaptively informed by the structural and interaction information in $\mathbf{E}$. After RMHA, $\mathbf{O}_i$ is passed to an MLP to update the atom representation $\mathbf{H}_i$, and the linear combination of $\mathbf{O}_i$ and $\mathbf{O}_j$ is used to update the pair representation $\mathbf{E}_{i,j}$. As Figure 2b illustrates, residual connections and adaLNs are included for improved performance.

Random Rotation Augmentation. Following AlphaFold3 (Abramson et al., 2024), we apply the same random rotation augmentation on both the input 3D coordinates ($\mathbf{x}^{(t)}$) and the target 3D coordinates ($\boldsymbol{\epsilon}^{(t)}$) to help DMT obtain equivariance to rotated inputs by learning. While (Wang et al., 2024) report decreased performance given random rotations, DMT benefits from it, potentially due to the improved neural architecture.

3.3 MoLlama Representations Improve DMT's 3D Conformer Prediction

We explore the transfer learning between molecular 1D sequences and 3D conformers. As Figure 3 illustrates, we leverage MoLlama's pretrained representation to improve DMT's 3D conformer prediction. This is achieved by our cross-modal projector and the corresponding training paradigm.

Cross-Modal Projector. This projector enables DMT to effectively leverage MoLlama for atom representation, addressing two challenges: (1) MoLlama uses causal self-attention, where each token only perceives preceding tokens, limiting the representation quality; and (2) SELFIES tokens do not map directly to individual atoms. Mitigating the first issue, we feed MoLlama's SELFIES representations into a single-layer bi-directional self-attention (Vaswani et al., 2017), expanding the receptive field for every SELFIES token. Further, we program the SELFIES-to-atom mapping using the SELFIES and RDKit software. For atoms corresponding to multiple SELFIES tokens, we obtain

its representation by mean pooling; for hydrogen atoms without corresponding SELFIES tokens, we use a learnable token as a replacement. The output of the SELFIES-to-atom mapping is then fed into an MLP and concatenated with DMT's original atom representations for 3D conformer prediction.

Training Strategy. As Figure 3b illustrates, we fine-tune a pretrained DMT to incorporate MoLlama representations, instead of training a new DMT from scratch using MoLlama representations, to save computation. Throughout the process, MoLlama uses LoRA tuning (Hu et al., 2021) to save memory. The training strategy consists of three stages. In the first stage, we train a standalone DMT without MoLlama until convergence. In the second stage, we attach MoLlama and the cross-modal projector to the pretrained DMT, keeping the DMT parameters frozen, and train for 10 epochs to warmup the random parameters in the projector and LoRA. This step prevents the gradients from the random parameters from distorting the pretrained DMT parameters (Kumar et al., 2022). In the final stage, we fine-tune the entire integrated model until convergence.

When incorporating MoLlama representations into DMT, we find that canonical SELFIES performs better than randomized SELFIES. This may be because bridging the gap between 1D MoLlama and 3D DMT is challenging, and using the fixed canonical representations leads faster convergence.

4 Experiment

In this section, we evaluate NEXT-Mol's performance on *de novo* 3D molecule generation, 3D conformer prediction, and conditional 3D molecule generation. We also present ablation studies to demonstrate the effectiveness of each component of NEXT-Mol.

4.1 Experimental Settings

Datasets. As Table 1 shows, we evaluate on the popular GEOM-DRUGS (Axelrod & Gomez-Bombarelli, 2022), GEOM-QM9 (Axelrod & Gomez-Bombarelli, 2022), and QM9-2014 (Ramakrishnan et al., 2014) datasets. Among them, we focus on GEOM-DRUGS, which is the most pharmaceutically relevant and largest one. Due to different tasks incorporating different dataset splits, we separately fine-tune NEXT-Mol for each task without sharing weights.

Table 1: Datasets for each task.

Task	Dataset
De novo 3D Mol Gen	GEOM-DRUGS, QM9-2014
3D Conformer Pred	GEOM-DRUGS, GEOM-QM9
Conditional 3D Mol Gen	QM9-2014

Baselines. For *de novo* and conditional 3D molecule genration tasks, we compare NEXT-Mol with baselines of CDGS (Huang et al., 2023a), JODO (Huang et al., 2024), MiDi (Vignac et al., 2023b), G-SchNet (Gebauer et al., 2019), G-SphereNet (Luo & Ji, 2022), E-NF (Garcia Satorras et al., 2021), EDM (Hoogeboom et al., 2022), MDM (Huang et al., 2023b), GeoLDM (Xu et al., 2023), EEGSDE (Bao et al., 2023), EQGAT-diff (Le et al., 2024), MolGPT (Bagal et al., 2021), and MolGen (Fang et al., 2024). For 3D conformer prediction, we report baseline performances of RDKit (Landrum, 2013), OMEGA (Hawkins, 2017), GeoMol (Ganea et al., 2021), GeoDiff (Xu et al., 2022), Torsional Diffusion (Jing et al., 2022), Particle Guidance (Corso et al., 2024), and MCF (Wang et al., 2024). More details on experimental settings are in Appendix D.

NEXT-Mol. Throughout the section, NEXT-Mol fine-tunes the pretrained 960M MoLlama for 1D molecule generation. We have trained two versions of DMT: DMT-B of 55 million parameters and DMT-L of 150 million. For the *de novo* and conditional 3D generation molecule tasks (*cf.* Section 4.2 and Section 4.4), NEXT-Mol uses DMT-B. DMT uses 100 sampling steps by default.

4.2 *De Novo* 3D Molecule Generation

Experimental Setting. Generating a complete 3D molecule involves generating the 2D molecular graph and the corresponding 3D conformer. Therefore, we evaluate both the predicted 2D molecular graphs (*i.e.,* 2D-Metric), and the predicted 3D coordinates (*i.e.,* 3D-Metric), following (Hoogeboom et al., 2022; Huang et al., 2024). 2D-Metrics can be roughly grouped into three types: (1) stability and validity: atom stability, molecule stability, and validity & completeness (V&C); (2) diversity: validity & uniqueness (V&U), and validity & uniqueness & novelty (V&U&N); and (3) distribution similarity between the generated molecules and the test set: similarity to nearest neighbor (SNN), fragment similarity (Frag), scaffold similarity (Scaf), and Fréchet ChemNet Distance

Table 2: Performances for *de novo* 3D molecule generation. * denotes our reproduced results using their source codes. Other baseline results are borrowed from (Huang et al., 2024). 2D-Metric evaluates the directly predicted 2D molecular graphs, whereas the 3D-Metric evaluates the predicted 3D coordinates or the 2D molecular graphs reconstructed from the 3D coordinates.

(a) Performances on the GEOM-DRUGS dataset.

2D-Metric	FCD↓	AtomStable	MolStable	V&C	V&U	V&U&N	SNN	Frag	Scaf
Train	0.251	1.000	1.000	1.000	1.000	0.000	0.585	0.999	0.584
MolGPT*	0.888	0.957	0.957	0.957	0.955	0.918	0.520	0.991	0.539
MolGen*	0.655	**1.000**	0.995	**1.000**	0.993	0.759	0.513	0.993	0.549
CDGS	22.051	0.991	0.706	0.285	0.285	0.285	0.262	0.789	0.022
JODO	2.523	**1.000**	0.981	0.874	0.905	0.902	0.417	0.993	0.483
MiDi*	7.054	0.968	0.822	0.633	0.654	0.652	0.392	0.951	0.196
EQGAT-diff*	6.310	0.999	0.998	0.959	0.993	0.702	0.368	0.986	0.147
NEXT-Mol, ours	**0.334**	**1.000**	**0.999**	**1.000**	**0.999**	**0.945**	**0.529**	**0.999**	**0.552**

3D-Metric	FCD↓	AtomStable	Bond length↓	Bond angle↓	Dihedral angle↓
Train	13.73	0.861	1.56E-04	1.81E-04	1.56E-04
EDM	31.29	0.831	4.29E-01	4.96E-01	1.46E-02
JODO	19.99	0.845	8.49E-02	1.15E-02	6.68E-04
MiDi*	23.14	0.750	1.17E-01	9.57E-02	4.46E-03
EQGAT-diff*	25.89	0.846	1.23E-01	5.29E-02	2.17E-03
NEXT-Mol, ours	**14.69**	**0.848**	**2.05E-02**	**8.18E-03**	**2.31E-04**

(b) Performances on the QM9-2014 dataset.

2D-Metric	FCD↓	AtomStable	MolStable	V&C	V&U	V&U&N	SNN	Frag	Scaf
Train	0.063	0.999	0.988	0.989	0.989	0.000	0.490	0.992	0.946
MolGPT*	0.461	0.975	0.975	0.975	0.936	0.763	0.523	0.958	0.923
MolGen*	0.085	**1.000**	0.988	**1.000**	0.955	0.479	0.500	0.988	0.934
CDGS	0.798	0.997	0.951	0.951	0.936	**0.860***	0.493	0.973	0.784
JODO	0.138	0.999	0.988	0.990	0.960	0.780*	0.522	0.986	0.934
MiDi*	0.187	0.998	0.976	0.980	0.954	0.769	0.501	0.979	0.882
EQGAT-diff*	2.157	1.000	0.972	1.000	0.996	0.695	0.479	0.949	0.707
NEXT-Mol, ours	**0.070**	**1.000**	**0.989**	**1.000**	**0.967**	0.802	**0.530**	**0.992**	**0.945**

3D-Metric	FCD↓	AtomStable	Bond length↓	Bond angle↓	Dihedral angle↓
Train	0.877	0.994	5.44E-04	4.65E-04	1.78E-04
E-NF	4.452	0.847	6.17E-01	4.20E-01	5.60E-03
G-SchNet	2.386	0.957	3.62E-01	7.27E-02	4.20E-03
G-SphereNet	6.659	0.672	1.51E-01	3.54E-01	1.29E-02
EDM	1.285	0.986	1.30E-01	1.82E-02	6.64E-04
MDM	4.861	0.992	2.74E-01	6.60E-02	2.39E-02
JODO	0.885	0.992	1.48E-01	1.21E-02	6.29E-04
MiDi*	1.100	0.983	8.96E-01	2.08E-02	8.14E-04
EQGAT-diff*	1.519	0.988	4.09E-01	1.91E-02	1.14E-03
NEXT-Mol, ours	**0.879**	**0.993**	**1.15E-01**	**7.32E-03**	**1.95E-04**

(FCD) (Polykovskiy et al., 2020). For 3D-Metrics, we follow (Hoogeboom et al., 2022) to evaluate the predicted 3D molecules by assessing atom stability, and FCD of the 2D molecular graphs reconstructed from predicted 3D coordinates. Additionally, 3D-Metrics includes the maximum mean discrepancy (MMD) (Gretton et al., 2012) for bond lengths, bond angles, and dihedral angles to evaluate geometric similarity to the test set. We also report training set performance for reference. The experimental results are presented in Table 2. We can observe that:

Obs. 1: NEXT-Mol Demonstrates Leading Performances for 3D Molecule Generation. It achieves the best performance across all metrics on GEOM-DRUGS, and achieves the best performance in 14 out of 15 metrics on QM9-2014. Although CDGS shows a higher novelty score on QM9-2014, it significantly underperforms NEXT-Mol for other metrics. This observation shows that NEXT-Mol is highly effective at generating chemically valid and diverse 3D molecular structures. Its strong performance on both large (*i.e.,* GEOM-DRUGS) and small (*i.e.,* QM9-2014) molecules highlights its robustness and potential as a foundation model for various tasks.

Table 3: 3D conformer prediction results. Baseline results are from (Jing et al., 2022; Corso et al., 2024; Wang et al., 2024). * denotes reproduction using their codes. -R←Recall and -P←Precision.

(a) Performances on the GEOM-DRUGS dataset. TD *w/* PG denotes torsional diffusion with particle guidance.

		COV-R (%)↑		AMR-R ↓		COV-P (%)↑		AMR-P ↓	
Method	Model Size	Mean	Median	Mean	Median	Mean	Median	Mean	Median
Model size ≤ 100M									
RDKit	-	38.4	28.6	1.058	1.002	40.9	30.8	0.995	0.895
OMEGA	-	53.4	54.6	0.841	0.762	40.5	33.3	0.946	0.854
GeoMol	0.3M	44.6	41.4	0.875	0.834	43.0	36.4	0.928	0.841
GeoDiff	1.6M	42.1	37.8	0.835	0.809	24.9	14.5	1.136	1.090
Torsional Diffusion	1.6M	72.7	80.0	0.582	0.565	55.2	56.9	0.778	0.729
TD *w/* PG	1.6M	77.0	82.6	0.543	0.520	68.9	78.1	0.656	0.594
TD *w/* PG*	1.6M	73.8	79.3	0.566	0.539	**65.2**	**70.8**	0.680	0.615
MCF-S	13M	79.4	87.5	0.512	0.492	57.4	57.6	0.761	0.715
MCF-B	64M	84.0	91.5	0.427	0.402	64.0	66.2	0.667	0.605
DMT-B, ours	55M	**85.4**	**92.2**	**0.401**	**0.375**	**65.2**	67.8	**0.642**	**0.577**
Model size > 100M									
MCF-L	242M	84.7	92.2	0.390	**0.247**	66.8	71.3	0.618	0.530
DMT-L, ours	150M	**85.8**	**92.3**	**0.375**	0.346	**67.9**	**72.5**	**0.598**	**0.527**

(b) Performances on the GEOM-QM9 dataset.

		COV-R (%)↑		AMR-R ↓		COV-P (%)↑		AMR-P ↓	
Method	Model size	Mean	Median	Mean	Median	Mean	Median	Mean	Median
RDKit	-	85.1	**100.0**	0.235	0.199	86.8	**100.0**	0.232	0.205
OMEGA	-	85.5	**100.0**	0.177	0.126	82.9	**100.0**	0.224	0.186
GeoMol	0.3M	91.5	**100.0**	0.225	0.193	86.7	**100.0**	0.270	0.241
GeoDiff	1.6M	76.5	**100.0**	0.297	0.229	50.0	33.5	0.524	0.510
Torsoinal Diffusion	1.6M	92.8	**100.0**	0.178	0.147	92.7	**100.0**	0.221	0.195
MCF-B	64M	95.0	**100.0**	0.103	0.044	93.7	**100.0**	0.119	0.055
DMT-B, ours	55M	**95.2**	**100.0**	**0.090**	**0.036**	**93.8**	**100.0**	**0.108**	**0.049**

Table 4: Incorporating MoLlama's 1D representations to improve DMT's 3D conformer prediction.

		COV-R (%)↑		AMR-R ↓		COV-P (%)↑		AMR-P ↓	
Dataset	Method	Mean	Median	Mean	Median	Mean	Median	Mean	Median
GEOM-DRUGS	DMT-B	85.4	**92.2**	0.401	0.375	65.2	67.8	0.642	0.577
	+MoLlama	**86.1**	92.1	**0.383**	**0.367**	**66.2**	**68.6**	**0.626**	**0.566**
	DMT-L	85.8	92.3	0.375	0.346	67.9	**72.5**	0.598	0.527
	+MoLLama	**87.1**	**93.0**	**0.360**	**0.334**	**68.1**	71.8	**0.595**	**0.525**
GEOM-QM9	DMT-B	95.2	**100.0**	0.090	**0.036**	93.8	**100.0**	0.108	0.049
	+MoLlama	**95.6**	**100.0**	**0.083**	**0.036**	**94.2**	**100.0**	**0.097**	**0.044**

Obs. 2: NEXT-Mol is Powerful in Capturing 1D/2D Molecular Characteristics, including SNN, Frag, Scaf, and FCD. Notably, it improves the FCD from 0.655 to 0.334 on GEOM-DRUGS, achieving a 49% relative improvement. This good performance is attributed to MoLlama's extensive pre-training, which lays a strong foundation for the subsequent 3D conformer prediction.

4.3 3D Molecular Conformer Prediction

Experimental Setting. The setting follows (Jing et al., 2022). Evaluation metrics include Average Minimum RMSD (AMR), which measures the distance between a predicted conformer and a ground truth, and Coverage (COV), which measures the proportion of predicted conformers that are sufficiently close to a ground truth. Due to a 2D molecule can have multiple ground truth and predicted conformers, we report both precision (comparing a prediction to its most similar ground truth) and recall (comparing a ground truth to its most similar prediction) for AMR and Coverage.

Obs. 3: DMT Demonstrates Leading Performance for 3D Conformer Prediction. Table 3 compares DMT and baselines for 3D conformer prediction. We can observe that DMT-B outperforms

Table 5: Performance of conditional 3D molecule generation on the QM9-2014 dataset. We report MAE ↓ between the desired properties and the predicted properties of the generated samples. Baseline results are from (Huang et al., 2024). We **bold** the best performance.

Method	μ (D)	α (Bohr^3)	C_v $\left(\frac{\text{cal}}{\text{mol}}\text{K}\right)$	$\varepsilon_{\text{HOMO}}$ (meV)	$\varepsilon_{\text{LUMO}}$ (meV)	$\Delta\varepsilon$ (meV)
EDM	1.123	2.78	1.065	371	601	671
EEGSDE	0.777	2.50	0.941	302	447	487
GeoLDM	1.108	2.37	1.025	340	522	587
JODO	0.628	1.42	0.581	226	256	335
NEXT-Mol, ours	**0.507**	**1.16**	**0.512**	**205**	**235**	**297**
L-Bound	0.043	0.09	0.040	39	36	65

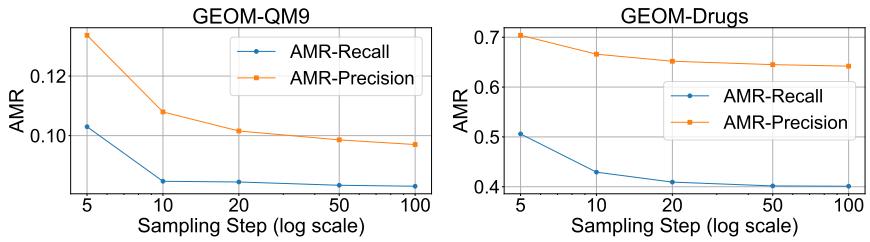

Figure 4: Effect of sampling steps on AMR↓ for 3D conformer prediction using DMT-B.

MCF-B, and DMT-L surpasses MCF-L, even though DMT-L is only 60% of the size of MCF-L. This improvement demonstrates that DMT can better utilize 2D molecular graph structures than MCF. Further, DMT-L improves upon DMT-B, demonstrating DMT's scalability. Both the improvements above are attributed to DMT's meticulously designed architecture, combining the power of scalability while effectively leveraging the full information of 2D molecular graphs.

Obs. 4: MoLlama's 1D Representation Improves DMT's 3D Conformer Prediction. As Table 4 shows, MoLlama enhances DMT on both GEOM-DRUGS and GEOM-QM9 datasets. This observation demonstrates the potential to leverage the abundant 1D molecule sequences to improve 3D generation and design tasks, mitigating their data scarcity issue. Further, this observation highlights MoLlama's value to generate expressive molecule representations for 3D tasks, beyond its 1D molecule generation ability. Although MoLlama is pretrained only on 1D molecules, we hypothesize that large-scale pretraining helps it develop chemical heuristics useful for 3D prediction.

4.4 Conditional 3D Molecule Generation with Quantum Chemical Properties

Adatping NEXT-Mol for Conditional Generation. We employ NEXT-Mol for conditional 3D molecule generation targeting quantum chemistry properties. To adapt NEXT-Mol to incorporate numerical conditions, the desired property values are encoded into vector embeddings using MLPs. These embeddings are prepended to the SELFIES sequences during MoLlama fine-tuning, serving as a soft-prompt to condition its output (Li & Liang, 2021), and are also fed into the DMT through the condition MLP module (*cf.* Figure 2). See Appendix D.4 for details of this methodology.

Remark. Quantum chemical properties (*e.g.,* HOMO-LUMO gap) often vary across a molecule's different 3D conformers. As a result, the 1D molecules generated by MoLlama alone cannot achieve errors lower than the average across a molecule's different conformers. To address this, we condition DMT on the desired property value when predicting the 3D conformer, enabling DMT to find the conformer that best matches the target property.

Experimental Settings. Following (Hoogeboom et al., 2022; Huang et al., 2024), we focus on six properties of heat capacity C_v, dipole moment μ, polarizability α, highest occupied molecular orbital energy ϵ_{HOMO}, lowest unoccupied molecular orbital energy ϵ_{LUMO}, and HOMO-LUMO gap $\Delta\epsilon$. For evaluation, we report the mean absolute error (MAE) between the desired property values and the predicted values of the generated molecules, using a property classifier network ϕ_c (Hoogeboom et al., 2022). QM9-2014's training set is split into two halves: D_a and D_b, each containing 50k molecules. ϕ_c is trained on D_a and NEXT-Mol is trained on D_b. We report ϕ_c's performance on D_b as the performance's lower-bound (L-Bound). Table 5 shows the results.

Table 6: Enhancing 3D molecule generation with MoLlama representations on GEOM-DRUGS.

Method	3D Pred.	AtomStable	MolStable	FCD↓	Bond length↓	Bond angle↓	Dihedral angle↓
NEXT-Mol	DMT-B	0.848	**0.027**	14.69	2.05E-02	8.18E-03	2.31E-04
	+MoLLama	**0.852**	**0.027**	**14.32**	**1.48E-02**	**8.08E-03**	**1.81E-04**

Table 7: Ablating random rotation augmentation for 3D conformer prediction on GEOM-QM9.

	COV-R (%)↑		AMR-R ↓		COV-P (%)↑		AMR-P ↓	
Method	Mean	Median	Mean	Median	Mean	Median	Mean	Median
DMT-B	**95.2**	**100.0**	**0.090**	**0.036**	**93.8**	**100.0**	**0.108**	**0.049**
w/o rand rot aug.	**95.2**	**100.0**	0.095	0.040	93.3	**100.0**	0.113	0.053

Table 8: Ablating randomized SELFIES augmentations for 1D molecule generation on QM9-2014.

2D metrics	AtomStable	MolStable	V&C	V&U	V&U&N	SNN	Frag	Scaf	FCD↓
MoLlama	**1.000**	**0.989**	**1.000**	**0.967**	**0.802**	**0.530**	**0.992**	**0.945**	**0.070**
w/o randomized aug.	**1.000**	0.988	**1.000**	0.948	0.395	0.491	0.989	0.939	0.074

Obs. 5: NEXT-Mol Outperforms Baselines for Conditional 3D Molecule Generation. The improvements are consistent and significant, demonstrating NEXT-Mol's ability to capture quantum chemical properties. This good performance is partially attributed to DMT, which finds the 3D conformer that best matches the desired property.

4.5 Ablation Study

Sampling Steps. As shown in Figure 4, we observe an improving trend in AMR for both recall and precision as the sampling steps increase from 5 to 100. The most significant improvements occur between 5 and 20 steps, with diminishing returns beyond 50 steps. This indicates that our model can half the inference cost by trading off a small amount of performance.

Enhancing 3D Molecule Generation with MoLlama Representations. For *de novo* 3D molecule generation, NEXT-Mol uses DMT-B without MoLlama for conformer prediction by default. Here we show that adding MoLlama representations to DMT-B further improves its performance on 3D-metrics. As Table 6 shows, the improvements are consistent, with significant gains in geometric measures (*i.e.,* bond lengths, angles, and dihedral angles), highlighting MoLlama's ability to enhance DMT's prediction on 3D geometry.

Random Rotation Augmentation. Table 7 shows that DMT benefits from random rotation augmentations. Unlike MCF (Wang et al., 2024), which relies on fixed canonical rotations, this is a key improvement because real data may be out-of-distribution and do not follow canonical rotations.

Random SELFIES Augmentation. As Table 8 shows, using randomized SELFIES augmentation significantly improves the novelty (*i.e.,* V&U&N) of the generated samples. It also improves other metrics, like SNN and FCD, highlighting its importance for 1D molecule generation.

5 Conclusion and Future Works

In this work, we presented NEXT-Mol, a foundation model for 3D molecule generation that integrated the strengths of 1D SELFIES-based LMs and 3D diffusion models. NEXT-Mol demonstrated leading performances in *de novo* 3D molecule generation, 3D conformer prediction, and conditional 3D molecule generation. These good performances are attributed to our focus on incorporating chemical inductive biases without compromising model scalability, and they highlight NEXT-Mol's promising potential as a foundation model in the field. Additionally, NEXT-Mol showed that transfer learning between 1D molecule sequences and 3D conformers can significantly improve 3D conformer prediction performance, underscoring the value of leveraging the abundant 1D molecular data to enhance 3D prediction tasks. Looking ahead, we plan to extend NEXT-Mol to process multiple molecular inputs, aiming to tackle structure-based molecule design and modeling interactions between small molecules and proteins or RNAs, with real-world applications in drug discovery.

6 Ethics Statement

Our research advances 3D molecule generation with the NExT-Mol model, aiming to enhance generative deep learning methods for molecular design. This work is primarily technical and foundational, with applications in drug discovery and materials science. We have carefully considered potential societal impacts and do not foresee any direct, immediate, or negative consequences. We are committed to the ethical dissemination of our findings and encourage their responsible use.

7 Reproducibility Statement

All the results in this work are reproducible. We provide all the necessary code to replicate our results in an anonymous GitHub repository https://anonymous.4open.science/r/NEXT-Mol. The repository includes environment configurations, run scripts, and other relevant materials.

We discuss the experimental settings for various tasks in Section 4, including details on parameters such as sampling steps. Additionally, detailed experimental settings are provided in Appendix D.

References

Josh Abramson, Jonas Adler, Jack Dunger, Richard Evans, Tim Green, Alexander Pritzel, Olaf Ronneberger, Lindsay Willmore, Andrew J Ballard, Joshua Bambrick, et al. Accurate structure prediction of biomolecular interactions with alphafold 3. *Nature*, pp. 1–3, 2024.

Walid Ahmad, Elana Simon, Seyone Chithrananda, Gabriel Grand, and Bharath Ramsundar. Chemberta-2: Towards chemical foundation models. *CoRR*, abs/2209.01712, 2022. doi: 10.48550/ARXIV.2209.01712. URL https://doi.org/10.48550/arXiv.2209.01712.

Josep Arús-Pous, Simon Johansson, Oleksii Prykhodko, Esben Jannik Bjerrum, Christian Tyrchan, Jean-Louis Reymond, Hongming Chen, and Ola Engkvist. Randomized SMILES strings improve the quality of molecular generative models. *J. Cheminformatics*, 11(1):71:1–71:13, 2019.

Simon Axelrod and Rafael Gomez-Bombarelli. Geom, energy-annotated molecular conformations for property prediction and molecular generation. *Scientific Data*, 9(1):185, 2022.

Jimmy Lei Ba. Layer normalization. *arXiv preprint arXiv:1607.06450*, 2016.

Viraj Bagal, Rishal Aggarwal, PK Vinod, and U Deva Priyakumar. Molgpt: molecular generation using a transformer-decoder model. *Journal of Chemical Information and Modeling*, 62(9):2064–2076, 2021.

Fan Bao, Min Zhao, Zhongkai Hao, Peiyao Li, Chongxuan Li, and Jun Zhu. Equivariant energy-guided SDE for inverse molecular design. In *ICLR*. OpenReview.net, 2023.

Jannis Born and Matteo Manica. Regression transformer enables concurrent sequence regression and generation for molecular language modelling. *Nat. Mac. Intell.*, 5(4):432–444, 2023.

Shaked Brody, Uri Alon, and Eran Yahav. How attentive are graph attention networks? In *The Tenth International Conference on Learning Representations, ICLR 2022, Virtual Event, April 25-29, 2022*. OpenReview.net, 2022. URL https://openreview.net/forum?id=F72ximsx7C1.

Gabriele Corso, Yilun Xu, Valentin De Bortoli, Regina Barzilay, and Tommi S. Jaakkola. Particle guidance: non-i.i.d. diverse sampling with diffusion models. In *ICLR*. OpenReview.net, 2024.

Tri Dao. Flashattention-2: Faster attention with better parallelism and work partitioning. In *The Twelfth International Conference on Learning Representations*, 2024. URL https://openreview.net/forum?id=mZn2Xyh9Ec.

Jacob Devlin, Ming-Wei Chang, Kenton Lee, and Kristina Toutanova. BERT: pre-training of deep bidirectional transformers for language understanding. In *NAACL-HLT*, pp. 4171–4186. Association for Computational Linguistics, 2019.

Yuanqi Du, Tianfan Fu, Jimeng Sun, and Shengchao Liu. Molgensurvey: A systematic survey in machine learning models for molecule design. *arXiv preprint arXiv:2203.14500*, 2022.

Peter Eckmann, Kunyang Sun, Bo Zhao, Mudong Feng, Michael K. Gilson, and Rose Yu. LIMO: latent inceptionism for targeted molecule generation. In *ICML*, volume 162 of *Proceedings of Machine Learning Research*, pp. 5777–5792. PMLR, 2022.

Yin Fang, Ningyu Zhang, Zhuo Chen, Lingbing Guo, Xiaohui Fan, and Huajun Chen. Domain-agnostic molecular generation with self-feedback. In *ICLR*. OpenReview.net, 2024.

Daniel Flam-Shepherd, Kevin Zhu, and Alán Aspuru-Guzik. Language models can learn complex molecular distributions. *Nature Communications*, 13(1):3293, 2022.

Gordon L Flynn. Substituent constants for correlation analysis in chemistry and biology. by corwin hansch and albert leo., 1980.

Octavian Ganea, Lagnajit Pattanaik, Connor W. Coley, Regina Barzilay, Klavs F. Jensen, William H. Green Jr., and Tommi S. Jaakkola. Geomol: Torsional geometric generation of molecular 3d conformer ensembles. In *NeurIPS*, pp. 13757–13769, 2021.

Victor Garcia Satorras, Emiel Hoogeboom, Fabian Fuchs, Ingmar Posner, and Max Welling. E (n) equivariant normalizing flows. *Advances in Neural Information Processing Systems*, 34:4181–4192, 2021.

Niklas Gebauer, Michael Gastegger, and Kristof Schütt. Symmetry-adapted generation of 3d point sets for the targeted discovery of molecules. *Advances in neural information processing systems*, 32, 2019.

Niklas WA Gebauer, Michael Gastegger, Stefaan SP Hessmann, Klaus-Robert Müller, and Kristof T Schütt. Inverse design of 3d molecular structures with conditional generative neural networks. *Nature communications*, 13(1):973, 2022.

Rafael Gómez-Bombarelli, Jennifer N Wei, David Duvenaud, José Miguel Hernández-Lobato, Benjamín Sánchez-Lengeling, Dennis Sheberla, Jorge Aguilera-Iparraguirre, Timothy D Hirzel, Ryan P Adams, and Alán Aspuru-Guzik. Automatic chemical design using a data-driven continuous representation of molecules. *ACS central science*, 4(2):268–276, 2018.

Arthur Gretton, Karsten M Borgwardt, Malte J Rasch, Bernhard Schölkopf, and Alexander Smola. A kernel two-sample test. *The Journal of Machine Learning Research*, 13(1):723–773, 2012.

Tomas Hansson, Chris Oostenbrink, and WilfredF van Gunsteren. Molecular dynamics simulations. *Current opinion in structural biology*, 12(2):190–196, 2002.

Paul C. D. Hawkins. Conformation generation: The state of the art. *J. Chem. Inf. Model.*, 57(8): 1747–1756, 2017.

Jonathan Ho, Ajay Jain, and Pieter Abbeel. Denoising diffusion probabilistic models. *Advances in neural information processing systems*, 33:6840–6851, 2020.

Emiel Hoogeboom, Victor Garcia Satorras, Clément Vignac, and Max Welling. Equivariant diffusion for molecule generation in 3d. In *ICML*, volume 162 of *Proceedings of Machine Learning Research*, pp. 8867–8887. PMLR, 2022.

Zhenyu Hou, Xiao Liu, Yukuo Cen, Yuxiao Dong, Hongxia Yang, Chunjie Wang, and Jie Tang. Graphmae: Self-supervised masked graph autoencoders. In *KDD*, pp. 594–604. ACM, 2022.

Edward J. Hu, Yelong Shen, Phillip Wallis, Zeyuan Allen-Zhu, Yuanzhi Li, Shean Wang, and Weizhu Chen. Lora: Low-rank adaptation of large language models. *CoRR*, abs/2106.09685, 2021.

Weihua Hu, Bowen Liu, Joseph Gomes, Marinka Zitnik, Percy Liang, Vijay Pande, and Jure Leskovec. Strategies for pre-training graph neural networks. In *ICLR*, 2020.

Chenqing Hua, Sitao Luan, Minkai Xu, Zhitao Ying, Jie Fu, Stefano Ermon, and Doina Precup. Mudiff: Unified diffusion for complete molecule generation. In *LoG*, volume 231 of *Proceedings of Machine Learning Research*, pp. 33. PMLR, 2023.

Han Huang, Leilei Sun, Bowen Du, and Weifeng Lv. Conditional diffusion based on discrete graph structures for molecular graph generation. In *Proceedings of the AAAI Conference on Artificial Intelligence*, pp. 4302–4311, 2023a.

Han Huang, Leilei Sun, Bowen Du, and Weifeng Lv. Learning joint 2-d and 3-d graph diffusion models for complete molecule generation. *IEEE Transactions on Neural Networks and Learning Systems*, 2024.

Lei Huang, Hengtong Zhang, Tingyang Xu, and Ka-Chun Wong. MDM: molecular diffusion model for 3d molecule generation. In *AAAI*, pp. 5105–5112. AAAI Press, 2023b.

Ross Irwin, Spyridon Dimitriadis, Jiazhen He, and Esben Jannik Bjerrum. Chemformer: a pre-trained transformer for computational chemistry. *Mach. Learn. Sci. Technol.*, 3(1):15022, 2022.

Wengong Jin, Regina Barzilay, and Tommi S. Jaakkola. Junction tree variational autoencoder for molecular graph generation. In *ICML*, volume 80 of *Proceedings of Machine Learning Research*, pp. 2328–2337. PMLR, 2018.

Wengong Jin, Kevin Yang, Regina Barzilay, and Tommi S. Jaakkola. Learning multimodal graph-to-graph translation for molecule optimization. In *ICLR (Poster)*. OpenReview.net, 2019.

Bowen Jing, Gabriele Corso, Jeffrey Chang, Regina Barzilay, and Tommi S. Jaakkola. Torsional diffusion for molecular conformer generation. In *NeurIPS*, 2022.

Diederik Kingma, Tim Salimans, Ben Poole, and Jonathan Ho. Variational diffusion models. *Advances in neural information processing systems*, 34:21696–21707, 2021.

Thomas N Kipf and Max Welling. Semi-supervised classification with graph convolutional networks. In *ICLR*, 2017.

Mario Krenn, Florian Häse, AkshatKumar Nigam, Pascal Friederich, and Alán Aspuru-Guzik. Self-referencing embedded strings (SELFIES): A 100% robust molecular string representation. *Mach. Learn. Sci. Technol.*, 1(4):45024, 2020.

Ananya Kumar, Aditi Raghunathan, Robbie Matthew Jones, Tengyu Ma, and Percy Liang. Fine-tuning can distort pretrained features and underperform out-of-distribution. In *International Conference on Learning Representations*, 2022. URL https://openreview.net/forum?id=UYneFzXSJWh.

Greg Landrum. Rdkit documentation. *Release*, 1(1-79):4, 2013.

Tuan Le, Julian Cremer, Frank Noé, Djork-Arné Clevert, and Kristof T. Schütt. Navigating the design space of equivariant diffusion-based generative models for de novo 3d molecule generation. In *ICLR*. OpenReview.net, 2024.

Xiang Lisa Li and Percy Liang. Prefix-tuning: Optimizing continuous prompts for generation. In *ACL/IJCNLP (1)*, pp. 4582–4597. Association for Computational Linguistics, 2021.

Zeming Lin, Halil Akin, Roshan Rao, Brian Hie, Zhongkai Zhu, Wenting Lu, Nikita Smetanin, Robert Verkuil, Ori Kabeli, Yaniv Shmueli, et al. Evolutionary-scale prediction of atomic-level protein structure with a language model. *Science*, 379(6637):1123–1130, 2023.

Haotian Liu, Chunyuan Li, Qingyang Wu, and Yong Jae Lee. Visual instruction tuning. *Advances in neural information processing systems*, 36, 2024.

Qi Liu, Miltiadis Allamanis, Marc Brockschmidt, and Alexander Gaunt. Constrained graph variational autoencoders for molecule design. *Advances in neural information processing systems*, 31, 2018.

Shengchao Liu, Hanchen Wang, Weiyang Liu, Joan Lasenby, Hongyu Guo, and Jian Tang. Pre-training molecular graph representation with 3d geometry. In *ICLR*. OpenReview.net, 2022.

Chengqiang Lu, Qi Liu, Chao Wang, Zhenya Huang, Peize Lin, and Lixin He. Molecular property prediction: A multilevel quantum interactions modeling perspective. In *The Thirty-Third AAAI Conference on Artificial Intelligence, AAAI 2019, The Thirty-First Innovative Applications of Artificial Intelligence Conference, IAAI 2019, The Ninth AAAI Symposium on Educational Advances in Artificial Intelligence, EAAI 2019, Honolulu, Hawaii, USA, January 27 - February 1, 2019*, pp. 1052–1060. AAAI Press, 2019. doi: 10.1609/AAAI.V33I01.33011052. URL https://doi.org/10.1609/aaai.v33i01.33011052.

Youzhi Luo and Shuiwang Ji. An autoregressive flow model for 3d molecular geometry generation from scratch. In *International conference on learning representations (ICLR)*, 2022.

Youzhi Luo, Keqiang Yan, and Shuiwang Ji. Graphdf: A discrete flow model for molecular graph generation. In *ICML*, volume 139 of *Proceedings of Machine Learning Research*, pp. 7192–7203. PMLR, 2021.

Sohir Maskey, Ali Parviz, Maximilian Thiessen, Hannes Stärk, Ylli Sadikaj, and Haggai Maron. Generalized laplacian positional encoding for graph representation learning. *arXiv preprint arXiv:2210.15956*, 2022.

Alexander Quinn Nichol and Prafulla Dhariwal. Improved denoising diffusion probabilistic models. In *International conference on machine learning*, pp. 8162–8171. PMLR, 2021.

OpenEye, Cadence Molecular Sciences. *OMEGA 5.0.1.3*. OpenEye, Cadence Molecular Sciences, Santa Fe, NM. http://www.eyesopen.com.

William Peebles and Saining Xie. Scalable diffusion models with transformers. In *Proceedings of the IEEE/CVF International Conference on Computer Vision*, pp. 4195–4205, 2023.

Ethan Perez, Florian Strub, Harm de Vries, Vincent Dumoulin, and Aaron C. Courville. Film: Visual reasoning with a general conditioning layer. In *AAAI*, pp. 3942–3951. AAAI Press, 2018.

Daniil Polykovskiy, Alexander Zhebrak, Benjamin Sanchez-Lengeling, Sergey Golovanov, Oktai Tatanov, Stanislav Belyaev, Rauf Kurbanov, Aleksey Artamonov, Vladimir Aladinskiy, Mark Veselov, Artur Kadurin, Simon Johansson, Hongming Chen, Sergey Nikolenko, Alan Aspuru-Guzik, and Alex Zhavoronkov. Molecular Sets (MOSES): A Benchmarking Platform for Molecular Generation Models. *Frontiers in Pharmacology*, 2020.

Mariya Popova, Olexandr Isayev, and Alexander Tropsha. Deep reinforcement learning for de novo drug design. *Science advances*, 4(7):eaap7885, 2018.

Mariya Popova, Mykhailo Shvets, Junier Oliva, and Olexandr Isayev. Molecularrnn: Generating realistic molecular graphs with optimized properties. *arXiv preprint arXiv:1905.13372*, 2019.

Raghunathan Ramakrishnan, Pavlo O Dral, Matthias Rupp, and O Anatole Von Lilienfeld. Quantum chemistry structures and properties of 134 kilo molecules. *Scientific data*, 1(1):1–7, 2014.

Zachary A Rollins, Alan C Cheng, and Essam Metwally. Molprop: Molecular property prediction with multimodal language and graph fusion. *Journal of Cheminformatics*, 16(1):56, 2024.

Vıctor Garcia Satorras, Emiel Hoogeboom, and Max Welling. E (n) equivariant graph neural networks. In *International conference on machine learning*, pp. 9323–9332. PMLR, 2021.

Kristof T Schütt, Huziel E Sauceda, P-J Kindermans, Alexandre Tkatchenko, and K-R Müller. Schnet–a deep learning architecture for molecules and materials. *The Journal of Chemical Physics*, 148(24), 2018.

Chence Shi, Minkai Xu, Zhaocheng Zhu, Weinan Zhang, Ming Zhang, and Jian Tang. Graphaf: a flow-based autoregressive model for molecular graph generation. In *ICLR*. OpenReview.net, 2020.

Gregor Simm, Robert Pinsler, and José Miguel Hernández-Lobato. Reinforcement learning for molecular design guided by quantum mechanics. In *International Conference on Machine Learning*, pp. 8959–8969. PMLR, 2020.

Hannes Stärk, Dominique Beaini, Gabriele Corso, Prudencio Tossou, Christian Dallago, Stephan Günnemann, and Pietro Lió. 3d infomax improves gnns for molecular property prediction. In Kamalika Chaudhuri, Stefanie Jegelka, Le Song, Csaba Szepesvári, Gang Niu, and Sivan Sabato (eds.), *International Conference on Machine Learning, ICML 2022, 17-23 July 2022, Baltimore, Maryland, USA*, volume 162 of *Proceedings of Machine Learning Research*, pp. 20479–20502. PMLR, 2022. URL https://proceedings.mlr.press/v162/stark22a.html.

Teague Sterling and John J. Irwin. ZINC 15 - ligand discovery for everyone. *J. Chem. Inf. Model.*, 55(11):2324–2337, 2015.

Mengying Sun, Jing Xing, Han Meng, Huijun Wang, Bin Chen, and Jiayu Zhou. Molsearch: Search-based multi-objective molecular generation and property optimization. In *KDD*, pp. 4724–4732. ACM, 2022.

Benjamin I Tingle, Khanh G Tang, Mar Castanon, John J Gutierrez, Munkhzul Khurelbaatar, Chinzorig Dandarchuluun, Yurii S Moroz, and John J Irwin. Zinc-22 a free multi-billion-scale database of tangible compounds for ligand discovery. *Journal of chemical information and modeling*, 63 (4):1166–1176, 2023.

Hugo Touvron, Louis Martin, Kevin Stone, Peter Albert, Amjad Almahairi, Yasmine Babaei, Nikolay Bashlykov, Soumya Batra, Prajjwal Bhargava, Shruti Bhosale, Dan Bikel, Lukas Blecher, Cristian Canton-Ferrer, Moya Chen, Guillem Cucurull, David Esiobu, Jude Fernandes, Jeremy Fu, Wenyin Fu, Brian Fuller, Cynthia Gao, Vedanuj Goswami, Naman Goyal, Anthony Hartshorn, Saghar Hosseini, Rui Hou, Hakan Inan, Marcin Kardas, Viktor Kerkez, Madian Khabsa, Isabel Kloumann, Artem Korenev, Punit Singh Koura, Marie-Anne Lachaux, Thibaut Lavril, Jenya Lee, Diana Liskovich, Yinghai Lu, Yuning Mao, Xavier Martinet, Todor Mihaylov, Pushkar Mishra, Igor Molybog, Yixin Nie, Andrew Poulton, Jeremy Reizenstein, Rashi Rungta, Kalyan Saladi, Alan Schelten, Ruan Silva, Eric Michael Smith, Ranjan Subramanian, Xiaoqing Ellen Tan, Binh Tang, Ross Taylor, Adina Williams, Jian Xiang Kuan, Puxin Xu, Zheng Yan, Iliyan Zarov, Yuchen Zhang, Angela Fan, Melanie Kambadur, Sharan Narang, Aurélien Rodriguez, Robert Stojnic, Sergey Edunov, and Thomas Scialom. Llama 2: Open foundation and fine-tuned chat models. *CoRR*, abs/2307.09288, 2023.

Ashish Vaswani, Noam Shazeer, Niki Parmar, Jakob Uszkoreit, Llion Jones, Aidan N. Gomez, Lukasz Kaiser, and Illia Polosukhin. Attention is all you need. In *NIPS*, pp. 5998–6008, 2017.

Clément Vignac, Igor Krawczuk, Antoine Siraudin, Bohan Wang, Volkan Cevher, and Pascal Frossard. Digress: Discrete denoising diffusion for graph generation. In *ICLR*. OpenReview.net, 2023a.

Clément Vignac, Nagham Osman, Laura Toni, and Pascal Frossard. Midi: Mixed graph and 3d denoising diffusion for molecule generation. In *ECML/PKDD (2)*, volume 14170 of *Lecture Notes in Computer Science*, pp. 560–576. Springer, 2023b.

Yuyang Wang, Jianren Wang, Zhonglin Cao, and Amir Barati Farimani. Molecular contrastive learning of representations via graph neural networks. *Nat. Mach. Intell.*, 4(3):279–287, 2022. doi: 10.1038/S42256-022-00447-X. URL https://doi.org/10.1038/s42256-022-00447-x.

Yuyang Wang, Ahmed A. A. Elhag, Navdeep Jaitly, Joshua M. Susskind, and Miguel Ángel Bautista. Swallowing the bitter pill: Simplified scalable conformer generation. In *ICML*. OpenReview.net, 2024.

David Weininger. Smiles, a chemical language and information system. 1. introduction to methodology and encoding rules. *J. Chem. Inf. Comput. Sci.*, 28(1):31–36, 1988.

Ruidong Wu, Fan Ding, Rui Wang, Rui Shen, Xiwen Zhang, Shitong Luo, Chenpeng Su, Zuofan Wu, Qi Xie, Bonnie Berger, et al. High-resolution de novo structure prediction from primary sequence. *BioRxiv*, pp. 2022–07, 2022.

Zhenqin Wu, Bharath Ramsundar, Evan N Feinberg, Joseph Gomes, Caleb Geniesse, Aneesh S Pappu, Karl Leswing, and Vijay Pande. Moleculenet: a benchmark for molecular machine learning. *Chemical science*, 9(2):513–530, 2018.

Yutong Xie, Chence Shi, Hao Zhou, Yuwei Yang, Weinan Zhang, Yong Yu, and Lei Li. MARS: markov molecular sampling for multi-objective drug discovery. In *ICLR*. OpenReview.net, 2021.

Keyulu Xu, Weihua Hu, Jure Leskovec, and Stefanie Jegelka. How powerful are graph neural networks? In *ICLR*, 2019.

Minkai Xu, Lantao Yu, Yang Song, Chence Shi, Stefano Ermon, and Jian Tang. Geodiff: A geometric diffusion model for molecular conformation generation. In *ICLR*. OpenReview.net, 2022.

Minkai Xu, Alexander S. Powers, Ron O. Dror, Stefano Ermon, and Jure Leskovec. Geometric latent diffusion models for 3d molecule generation. In *ICML*, volume 202 of *Proceedings of Machine Learning Research*, pp. 38592–38610. PMLR, 2023.

Kevin Yang, Kyle Swanson, Wengong Jin, Connor W. Coley, Philipp Eiden, Hua Gao, Angel Guzman-Perez, Timothy Hopper, Brian Kelley, Miriam Mathea, Andrew Palmer, Volker Settels, Tommi S. Jaakkola, Klavs F. Jensen, and Regina Barzilay. Analyzing learned molecular representations for property prediction. *J. Chem. Inf. Model.*, 59(8):3370–3388, 2019. doi: 10.1021/ACS.JCIM.9B00237. URL https://doi.org/10.1021/acs.jcim.9b00237.

Jiaxuan You, Bowen Liu, Zhitao Ying, Vijay Pande, and Jure Leskovec. Graph convolutional policy network for goal-directed molecular graph generation. *Advances in neural information processing systems*, 31, 2018.

Atakan Yüksel, Erva Ulusoy, Atabey Ünlü, Gamze Deniz, and Tunca Dogan. Selformer: Molecular representation learning via SELFIES language models. *CoRR*, abs/2304.04662, 2023.

Peiyuan Zhang, Guangtao Zeng, Tianduo Wang, and Wei Lu. Tinyllama: An open-source small language model. *CoRR*, abs/2401.02385, 2024.

Zaixi Zhang, Yaosen Min, Shuxin Zheng, and Qi Liu. Molecule generation for target protein binding with structural motifs. In *ICLR*. OpenReview.net, 2023.

Yanli Zhao, Andrew Gu, Rohan Varma, Liang Luo, Chien-Chin Huang, Min Xu, Less Wright, Hamid Shojanazeri, Myle Ott, Sam Shleifer, et al. Pytorch fsdp: experiences on scaling fully sharded data parallel. *arXiv preprint arXiv:2304.11277*, 2023.

Xiaofan Zheng and Yoichi Tomiura. A bert-based pretraining model for extracting molecular structural information from a smiles sequence. *Journal of Cheminformatics*, 16(1):71, 2024.

Gengmo Zhou, Zhifeng Gao, Qiankun Ding, Hang Zheng, Hongteng Xu, Zhewei Wei, Linfeng Zhang, and Guolin Ke. Uni-mol: A universal 3d molecular representation learning framework. In *ICLR*. OpenReview.net, 2023.

A LIMITATIONS

NEXT-Mol has several limitations that have not been addressed due to our limited computational resources and other technical challenges. We outline these limitations below:

Explore Randomized SELFIES Data Augmentation in Pretraining. Although randomized SELFIES augmentation shows promising results when fine-tuning MoLlama for 1D molecule generation, we do not use this augmentation technique during pretraining due to our limited computational resources. We believe applying this technique in pretraining could lead to different outcomes. We leave this exploration for future work.

Explore Pretrained Molecular Large LM with Bi-directional Self-Attention. MoLlama uses causal self-attention, where each token can only attend to previous tokens. While this approach is a good fit for 1D molecule generation, it constrains MoLlama's potential for molecule representation learning. To mitigate this issue, we have attached a bi-directional self-attention layer after MoLlama (*cf.* Figure 3). However, a more natural solution would be to use a molecular LM with built-in bi-directional self-attention. Due to resource constraints, we do not pursue this, and existing works are often limited in scale (Irwin et al., 2022; Zheng & Tomiura, 2024). We hope this work draws more attention to this area and encourages the development of more foundation models for biochemistry.

Explore NEXT-Mol for Struture-based Molecule Generation. We do not explore NEXT-Mol for structure-based molecule generation (Zhang et al., 2023) due to the limited scope of this work. However, NEXT-Mol could be extended for this task by conditioning the generation process on the structural embeddings of target pockets, potentially using techniques like cross-attention, adaptive layer normalization (Peebles & Xie, 2023), or soft-prompting (Li & Liang, 2021). We leave this exploration for future work.

Limited Exploration on Diffusion Guidance. Our DMT model utilizes i.i.d. sampling, without exploring advanced sampling method like classifier guidance () and particle guidance (Corso et al., 2024). However, particle guidance demonstrates that a well-tuned guidance method can improve the conformer prediction by 10% precision. This is because the 3D molecular conformational space is large, and a guidance method with appropriate chemical inductive bias can improve the sampling efficiency. We leave this exploration as a future work.

Computational Cost when Incorporating MoLlama for 3D Conformer Prediction. Incorporating MoLlama, a large LM with 960M parameters, increases training time. For example, training DMT-B alone (55M parameters) takes 52 seconds per epoch on an A100 GPU, while DMT-B *with* MoLlama takes 210 seconds. We mitigated this problem by using a pretrained DMT-B, instead of training it from scratch, to reduce the training epochs when incorporating MoLlama. Yet, we will need improvement when transferring 1D representations from a large LM.

Quadratic Memory Complexity of DMT's Pair Representation. This pair representation incurs an additional $O(N^2)$ GPU memory cost than the standard transformer, compared to the standard transformer's $O(N)$ memory complexity when using FlashAttention, where N is the node number of molecular graphs. While we encountered no memory issues on the GEOM-DRUGS dataset (molecules with hundreds of nodes), this could be a bottleneck for molecules with thousands of nodes. Potential solutions include smaller batch sizes and model parallelism.

B MORE EXPERIMENTAL RESULTS

B.1 ABLATION STUDY

Ablating MoLlama Pretraining. As Table 9 shows, pretraining significantly improves MoLlama's performances on the 1D distribution similarity metrics of SNN, Scaf and FCD, but slightly decreases novelty score (V&U&N). This may be because the model without pretraining prefers a more random sampling, increasing the novelty but reducing the similarity to the desired molecule distribution. Pretraining does not significantly influence stability and validity measures, because they are mostly guaranteed by the SELFIES representations.

Table 9: Ablation study for the MoLlama pretraining for 1D molecule generation on the GEOM-DRUGS dataset.

Method	AtomStable	MolStable	V&C	V&U	V&U&N	SNN	Frag	Scaf	FCD↓
MoLlama	**1.000**	**0.999**	**1.000**	**0.999**	0.945	**0.529**	**0.999**	**0.552**	**0.334**
w/o pretraining	**1.000**	0.995	**1.000**	**0.999**	**0.974**	0.495	**0.999**	0.534	0.586

Table 10: Molecule property regression results on four MoleculeNet datasets (Wu et al., 2018). Baseline results are from (Rollins et al., 2024). Lower↓ is better.

Method	FreeSolv (RMSE)	ESOL (RMSE)	Lipo (RMSE)	QM7 (MAE)
GNN-based methods				
RF (Wang et al., 2022)	2.03±0.22	1.07±0.19	0.88±0.04	122.7±4.2
SVM (Wang et al., 2022)	3.14±0.00	1.50±0.00	0.82±0.00	156.9±0.0
GCN (Kipf & Welling, 2017)	2.87±0.14	1.43±0.05	0.85±0.08	122.9±2.2
GATv2 (Brody et al., 2022)	3.14±0.00	1.41±0.00	0.89±0.00	113.3±0.0
GIN (Xu et al., 2019)	2.76±0.18	1.45±0.02	0.85±0.07	124.8±0.7
SchNet (Schütt et al., 2018)	3.22±0.76	1.05±0.06	0.91±0.10	74.2±6.0
3D Infomax (Stärk et al., 2022)	2.23±0.26	0.95±0.04	0.74±0.01	-
MGCN (Lu et al., 2019)	3.35±0.01	1.27±0.15	1.11±0.04	77.6±4.7
D-MPNN (Yang et al., 2019)	2.18±0.91	0.98±0.26	0.65±0.05	105.8±13.2
Pretrained GNN-based methods				
Pretrain-GNN (Hu et al., 2020)	2.83±0.12	1.22±0.02	0.74±0.00	110.2±6.4
MolCLR (Wang et al., 2022)	2.20±0.20	1.11±0.01	0.65±0.08	87.2±2.0
LM-based methods				
ChemBERTa-2 (Ahmad et al., 2022)	2.047±0.00	0.889±0.00	0.798±0.00	172.8±0.00
MolPROP (Rollins et al., 2024)	1.70±0.09	0.777±0.02	0.733±0.02	151.8±10.0
MoLlama, ours	**1.59±0.04**	**0.740±0.01**	**0.627±0.01**	**63.5±1.6**

B.2 Molecule Property Prediction Results for MoLlama

Experimental Settings. To evaluate MoLlama's capabilities beyond 1D molecule generation, we apply it to molecular property prediction tasks, highlighting the quality of its molecular representations. Following the setup in (Rollins et al., 2024), we fine-tune MoLlama on four MoleculeNet (Wu et al., 2018) datasets: FreeSolv, ESOL, Lipo, and QM7. We adopt the same experimental settings and dataset splits as (Rollins et al., 2024), reporting mean performance and standard deviation over 10 random seeds. For each run, MoLlama is trained for 100 epochs, with test performance selected based on the validation dataset. We use a fixed learning rate of 1e-4 with the AdamW optimizer, and fine-tune MoLlama using LoRA (Hu et al., 2021) (LoRA $r = 8$ and $\alpha = 32$) applied to all linear layers of the model. Following Section 3.3, we attach a single-layer bi-directional self-attention layer after MoLlama to improve its encoding ability. After that, we apply a linear layer on the mean embedding of all molecule tokens for property prediction.

Observation. As shown in Table 10, MoLlama significantly outperforms baseline methods, achieving relative improvements of 6.5%, 4.7%, 3.5%, and 16.9% on the FreeSolv, ESOL, Lipo, and QM7 datasets, respectively. Notably, our baselines include LM-based, GNN-based, and pretrained GNN-based methods, and MoLlama's better performance demonstrates its advantages derived from the extensive pretraining.

B.3 Influence of Hyperparameters

Different Noise Schedules at Inference Time. We test DMT-B's robustness to different noise schedulers at inference, using two representative options: the linear (Ho et al., 2020) and polynomial (Hoogeboom et al., 2022) schedulers. The original noise scheduler, based on the cosine function, follows (Nichol & Dhariwal, 2021). In this study, we use the existing DMT-B checkpoint without retraining the model with these new schedulers, so the results are suboptimal.

Table 11: DMT-B's 3D conformer prediction performances on the GEOM-DRUGS dataset when using different noise schedulers at inference time.

	COV-R (%) ↑		AMR-R ↓		COV-P (%) ↑		AMR-P ↓	
Noise schedule	Mean	Median	Mean	Median	Mean	Median	Mean	Median
linear	62.7	62.7	0.648	0.634	60.3	60.6	0.726	0.624
cosine, original	85.4	92.2	0.401	0.375	65.2	67.8	0.642	0.577
polynomial	84.9	91.7	0.454	0.421	64.5	66.2	0.685	0.619

Table 12: DMT-B's 3D conformer prediction performances on the GEOM-DRUGS dataset when using different batch sizes.

	COV-R (%) ↑		AMR-R ↓		COV-P (%) ↑		AMR-P ↓	
Batch size	Mean	Median	Mean	Median	Mean	Median	Mean	Median
128	85.5	92.4	0.395	0.366	65.1	68.0	0.644	0.575
256, original	85.4	92.2	0.401	0.375	65.2	67.8	0.642	0.577
512	85.1	92.0	0.410	0.377	64.9	67.7	0.645	0.582

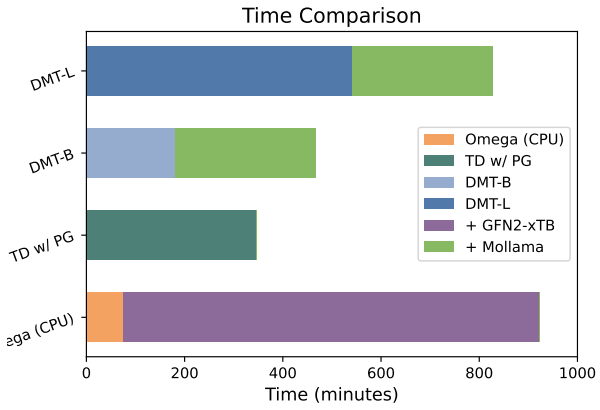

Figure 5: Comparison of conformer generation time on the test set of the GEOM-Drugs dataset using various methods.

Observation. As shown in Table 11, the polynomial scheduler achieves performance close to the cosine scheduler, likely because their curve shapes are similar. However, the linear scheduler results in a significant performance drop, suggesting that retraining DMT-B with the linear scheduler is necessary to achieve better results.

The Influence of Batch Size to 3D Conformer Prediction. We evaluate the performance of DMT-B with different batch sizes. The original batch size of 256 was chosen to maximize GPU utilization. To assess the impact of batch size, we tested two variations: (1) reducing the batch size to 128, and (2) increasing it to 512 using gradient accumulation.

Observation. As shown in Table 12, the performance with a 512 batch size is slightly worse than the original model. This is likely due to underfitting caused by fewer training steps. We keep the number of training epochs the same as the original experiment (256 batch size), therefore the larger batch size results in fewer gradient updates, leading to reduced model performance. Other than this observation, using the 128 batch size does not lead to significant difference than the original model.

B.4 Computational Time Comparison

We conducted a time comparison between our model and representative baselines for conformer generation on the test set of the GEOM-Drugs dataset, which includes 1000 molecules. The base-

Table 13: 3D Molecule stability performances. * denotes our reproduced results.

(a) GEOM-DRUGS dataset.

3D-Metric	MolStable
Train	0.953
E-NF	0.045
G-SchNet	0.681
G-SphereNet	0.134
EDM	0.817
MDM	0.896
JODO	0.934
MiDi*	0.842
EQGAT	0.889
NExT-Mol, ours	**0.946**

(b) QM9-2014 dataset.

3D-Metric	MolStable
Train	0.028
EDM	0.002
JODO	0.010
MiDi*	0.003
EQGAT	0.025
NExT-Mol, ours	**0.027**

lines include the OpenEye Omega (OpenEye, Cadence Molecular Sciences), TD w/ PG (Corso et al., 2024), and xTB[1]. The results are shown in Figure 5.

These experiments were performed on a platform with an 8-core Intel Xeon Processor@2.90GHz CPU and an NVIDIA A100 GPU and the time is measured in minutes and seconds. Please note that the Omega and xTB are run on the CPU only, while DMT and Mollama are run on the GPU. So the results may vary depending on the hardware.

B.5 3D Molecular Stability Performance

We do not report the 3D molecule stability metric (Hoogeboom et al., 2022) in the main part of this work, because this metric presents a significant limitation on the GEOM-DRUGS dataset, showing only 2.8% for the ground truth training set. We present the results here for backup purposes.

B.6 Visualization of Random Samples

Visualizations of complete molecules sampled from NEXT-Mol on GEOM-Drugs and QM9 are shown in Figure 6 and Figure 7, respectively. These samples are randomly selected to illustrate the diversity and effectiveness of our model. The visualization includes 1D SELFIES sequences, 2D molecular graphs, and 3D conformers highlighting the spatial arrangement of atoms within the molecules. Notably, in the complex GEOM-Drugs dataset, NEXT-Mol demonstrates its robustness by consistently generating molecules without disconnected components and effectively preserving the stable geometric planes of aromatic ring structures. These visualizations not only demonstrate the fidelity of the molecules generated by NEXT-Mol with 1D SELFIES sequences along with 3D spatial coordinates, but also emphasize the ability of our model to produce stable and chemically valid conformers accommodating a wide range of molecular weights.

C Further Details on Methodology

C.1 1D Molecule Generation with Molecular Llama LM

Data Preparation. Following (Irwin et al., 2022), we collect 1.8 billion molecules from the ZINC-15 database (Sterling & Irwin, 2015), significantly more than the 100 million molecules used in previous studies (Irwin et al., 2022; Fang et al., 2024). We keep only molecules with molecular weight$\leq$500 Daltons and LogP$\leq$5 (Flynn, 1980), and transform them into SELFIES (Krenn et al., 2020) sequences. After canonicalizing the SELFIES and removing hydrogen atoms, the dataset contains 90 billion tokens. We further filter the molecules in the valid and test sets of the GEOM-QM9 and GEOM-DRUGS datasets (Axelrod & Gomez-Bombarelli, 2022) and randomly sampled 1% of the remaining data as the validation set.

[1] https://xtb-docs.readthedocs.io/en/latest/

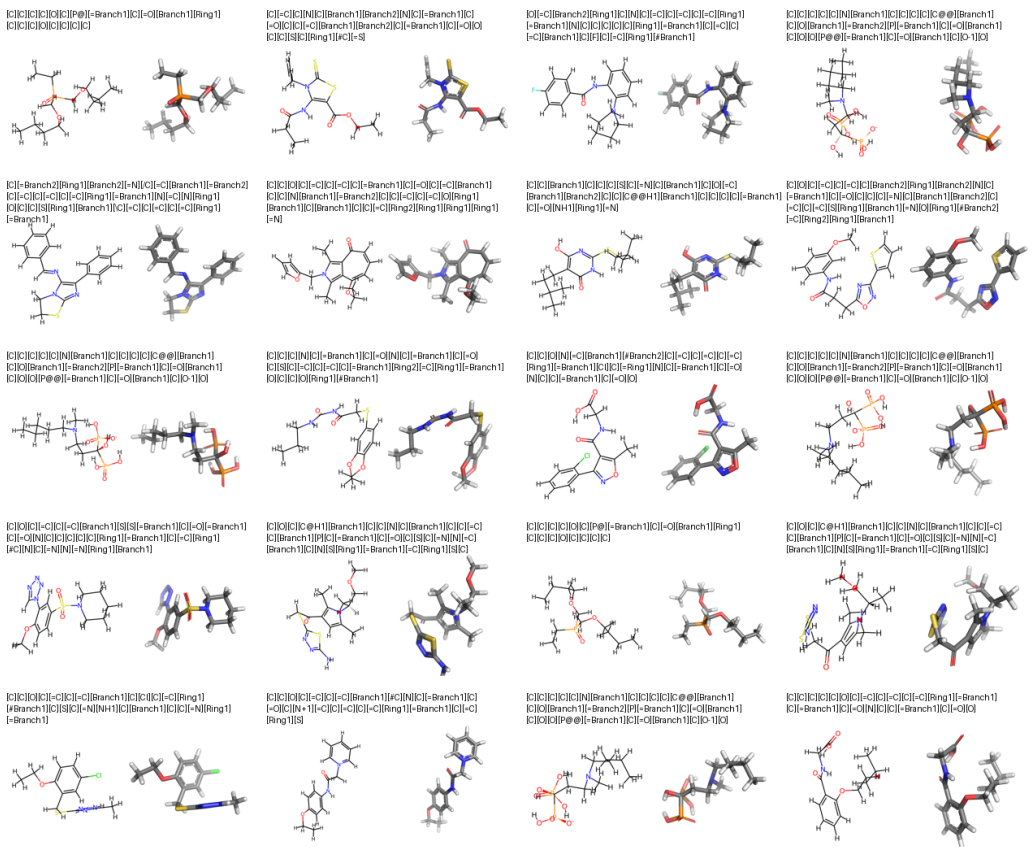

Figure 6: Visualization of random samples generated by NEXT-Mol trained on GEOM-DRUGS.

Table 14: Hyperparameter for pretraining MoLlama.

hidden size	2048	hidden act	silu
intermediate size	5632	batch size	512
max position embeddings	512	warmup steps	2000
num attention heads	32	min lr	4.00E-05
num hidden layers	22	init lr	4.00E-04
num key value heads	4	weight decay	1.00E-01
n query groups	4	grad clip	1.0

Randomized SELFIES Augmentation Details. In order to generate randomized SELFIES, we first generate the randomized SMILES (Weininger, 1988), and transform the SMILES into SELFIES. We follow (Arús-Pous et al., 2019) for the implementation details of random SMILES, and use a restricted random sampling of SMILES. Similarly, we also generate canonical SELFIES by transforming canonical SMILES.

Pretraining Details. We train MoLlama from scratch for 1D molecule generation using a next-token prediction objective. The code and hyperparameters are based on (Zhang et al., 2024), utilizing Flash-Attention (Dao, 2024) and FSDP (Zhao et al., 2023) for faster training. We use a max context length of 512, concatenating multiple SELFIES sequences into the same context, with any overflow trimmed and used in the next context. We use the AdamW optimizer and a scheduler with linear warmup and cosine decay. The key parameters are included in Table 14. We train the model for 555k global steps. The training was done on 4 NVIDIA A100-40G GPUs and took approximately two weeks. The training log is shown in Figure 8.

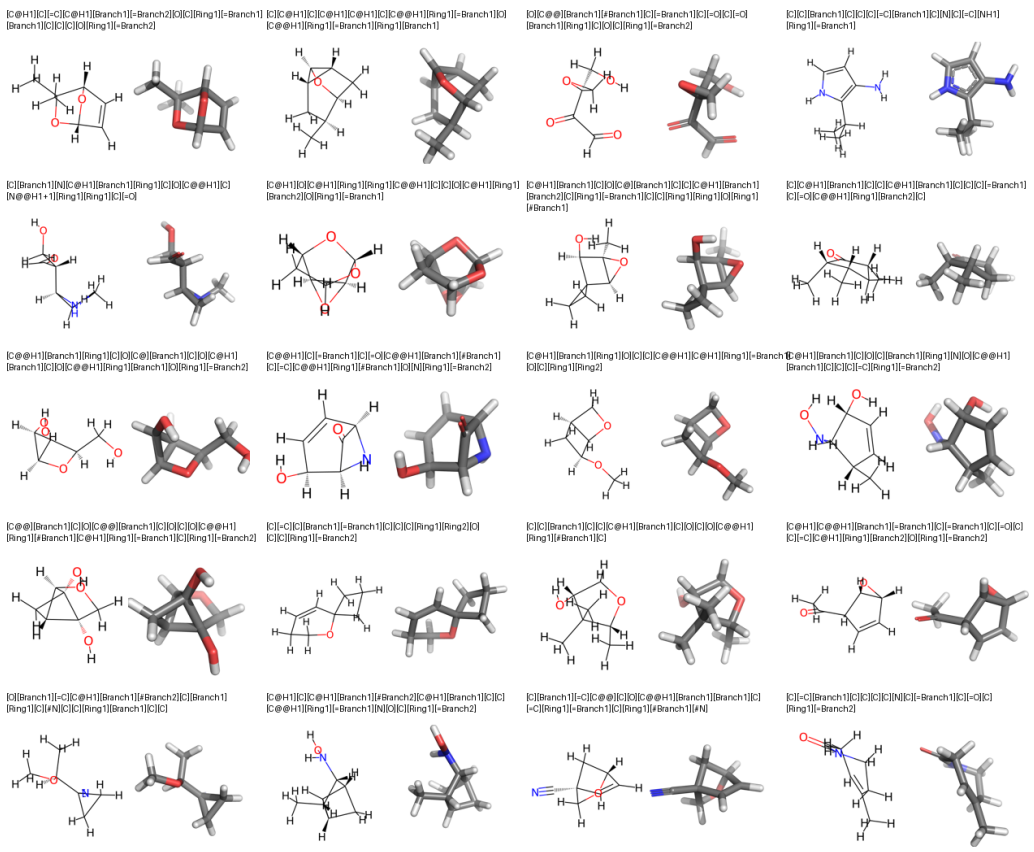

Figure 7: Visualization of random samples generated by NEXT-Mol trained on QM9-2014.

On the Advantages of Acheving 100% Validity beyond Validity Itself. We employ the 1D SELFIES representation for LM training. Here we elaborate on the other advantages beyond 100% validity, which are also crucial for real-world applications:

- **Improving validity could improve other 2D metrics, like SNN, Frag, and Scaf.** These metrics measure the distributional similarity of 2D molecular structures of valid molecules. If a model still generate invalid molecules, it is likely the model does not capture the true target distribution, which contain only valid molecules. 100% validity helps the model learn from and sample from the valid molecular structures, which is essential for molecule generation tasks. This is demonstrated by our improved FCD, SNN, Frag, and Scaf metrics in Table 2.
- **Improving validity could improve 3D geometry learning.** The improved validity also leads to better learning of 3D molecular geometry, because it grounds 3D structure prediction on valid 2D structures. Other joint 2D and 3D prediction methods (Huang et al., 2024; Vignac et al., 2023b) can easily encounter invalid 2D structures when sampling 3D structures, therefore leads to worse 3D structure prediction. This is demonstrated by NEXT-Mol's significant improvements in geometry similarity metrics (*e.g.,* bond angle and bond length) in Table 2.

C.2 3D Conformer Prediction with Diffusion Molecular Transformer

Diffusion Process. Here we elaborate on the details of our diffusion process. Following (Nichol & Dhariwal, 2021; Huang et al., 2024), we use the cosine scheduler controlling the noise scale for the diffusion process:

$$\bar{\alpha}_t = \frac{f(t)}{f(0)}, \quad f(t) = \cos\left(\frac{t+s}{1+s} \cdot \frac{\pi}{2}\right), \tag{5}$$

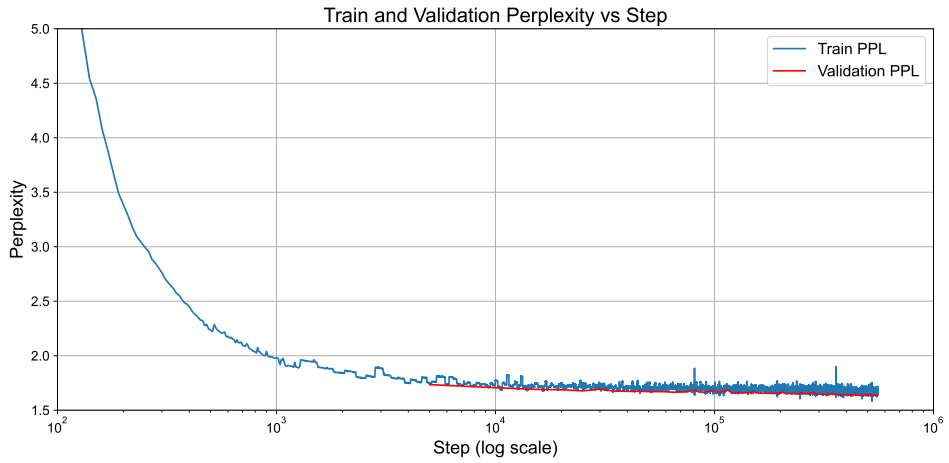

Figure 8: Visualization of MoLlama's training and validation PPL log during pretraining.

where $t \in (0, 1]$ is the time step, and s is a hyperparameter empirically set to 0.008, following (Nichol & Dhariwal, 2021).

Our pseudo codes for training and sampling are shown in Algorithm 1 and Algorithm 2 below. Following (Ho et al., 2020), we have the following hyperparameters used in the pseudo-codes for training and sampling:

$$\alpha^{(t)} = \bar{\alpha}^{(t)}/\bar{\alpha}^{(t-1)}, \quad \sigma^{(t)} = \sqrt{1 - \alpha^{(t)}}. \tag{6}$$

Algorithm 1 Training

$t \sim \mathcal{U}(0, 1]$ {Sample a time step}
$G^{(0)} = (\mathbf{x}^{(0)}, \mathbf{h}, \mathbf{e}) \sim$ Training Set {Sample a 3D molecule}
$\mathbf{x}^{(0)} \leftarrow \mathbf{x}^{(0)} - \bar{\mathbf{x}}^{(0)}$ {Centering molecule coordinates}
$\mathbf{x}^{(0)} \leftarrow \mathbf{x}^{(0)}R$, where $R \in SO(3)$ is randomly sampled {Random rotation augmentation}
$\boldsymbol{\epsilon}^{(t)} \sim \mathcal{N}(\mathbf{0}|\mathbf{I})$
$\mathbf{x}^{(t)} = \sqrt{\bar{\alpha}^{(t)}}\mathbf{x}^{(0)} + \sqrt{1 - \bar{\alpha}^{(t)}}\boldsymbol{\epsilon}^{(t)}$ {Forward diffusion}
$G^{(t)} \leftarrow (\mathbf{x}^{(t)}, \mathbf{h}, \mathbf{e})$
Minimize loss $\mathcal{L} = ||\boldsymbol{\epsilon}^{(t)} - \text{DMT}(G^{(t)}, t)||_2^2$

Algorithm 2 Sampling 3D Conformers

Require: time steps $\{t_i\}_{i=1}^{M}$, a 2D molecular graph $G_{\text{2D}} \leftarrow (\mathbf{h}, \mathbf{e})$
$\mathbf{x}^{(t_1)} \sim \mathcal{N}(\mathbf{0}, \mathbf{I})$ {Set the initial noise conformer}
for $i \leftarrow 1$ to M **do**
  $t \leftarrow t_{i-1}$, $s \leftarrow t_i$ {Set time step}
  $G^{(t)} \leftarrow (\mathbf{x}^{(t)}, \mathbf{h}, \mathbf{e})$
  $\mathbf{z} \sim \mathcal{N}(\mathbf{0}, \mathbf{I})$ if $i < M$ else $\mathbf{z} = \mathbf{0}$
  $\mathbf{x}^{(s)} = \frac{1}{\sqrt{\alpha_t}}\left(\mathbf{x}^{(t)} - \frac{1-\alpha^{(t)}}{\sqrt{1-\bar{\alpha}^{(t)}}}\text{DMT}(G^{(t)}, t)\right) + \sigma^{(t)}\mathbf{z}$ {Update conformer}
end for
return $\mathbf{x}^{(M)}$

RMHA. Here we define the multi-head version of RMHA. Similar to the single-head version, we first generate the queries, keys, and values for atom representation $\mathbf{H}$, and generate the queries and values for pair representation $\mathbf{E}$:

$$[\mathbf{Q};\mathbf{K};\mathbf{V}] = [\mathbf{W}_q;\mathbf{W}_k;\mathbf{W}_v]\mathbf{H}^\top, \quad (7) \qquad [\mathbf{Q}^E;\mathbf{V}^E] = \tanh([\mathbf{W}_{eq};\mathbf{W}_{ev}]\mathbf{E}^\top), \quad (8)$$

Subsequently, we define the Relational-Attention (R-Attention) module, which is the combination of Equation 3 and Equation 4:

$$\mathbf{O} = \text{R-Attention}(\mathbf{Q},\mathbf{K},\mathbf{V},\mathbf{Q}^E,\mathbf{V}^E), \quad (9)$$

$$\text{where } \mathbf{O}_i = \sum_{j=1}^{N} a_{i,j}(\mathbf{V}^E_{i,j} \odot \mathbf{V}_j), \quad (10)$$

$$a_{i,j} = \text{softmax}_j\left(\frac{(\mathbf{Q}^E_{i,j} \odot \mathbf{Q}_i)\mathbf{K}_j^\top}{\sqrt{d}}\right). \quad (11)$$

After this, the muli-head version of RMHA can be written as:

$$\text{RMHA}(\mathbf{Q},\mathbf{K},\mathbf{V},\mathbf{Q}^E,\mathbf{V}^E) = \text{Concat}(\mathbf{O}^1,...,\mathbf{O}^h)\mathbf{W}_o \quad (12)$$

$$\text{where } \mathbf{O}^f = \text{R-Attention}(\mathbf{W}_{qf}\mathbf{Q},\mathbf{W}_{kf}\mathbf{K},\mathbf{W}_{vf}\mathbf{V},\mathbf{W}_{eqf}\mathbf{Q}^E,\mathbf{W}_{evf}\mathbf{V}^E), \quad (13)$$

where h is the number of head; $f \in [1,h]$; $\mathbf{W}_o$ is the linear projector combining outputs of different heads; and $\mathbf{W}_{qf}$, $\mathbf{W}_{kf}$, and $\mathbf{W}_{vf}$ are linear projectors for the f-th head of atom representations; and $\mathbf{W}_{eqf}$ and $\mathbf{W}_{eqf}$ are linear projectors for the f-th head of the pair representation.

C.3 MoLLaMA Representations Improve DMT's 3D Conformer Prediction

Details of SELFIES-to-Atom Mapping. The mapping process is not straightforward with existing software, so we have to manually code a significant portion. For details on the full implementation, please refer to our code. In brief, the SELFIES software provides a mapping between SELFIES and SMILES tokens, and RDKit gives the atom order when generating SMILES. We manually convert this atom order into a mapping between SMILES and atom indices, then combine the SELFIES-to-SMILES and SMILES-to-atom mappings into the SELFIES-to-atom mapping. Additionally, we handle missing hydrogen atoms in both SMILES and SELFIES during the mapping process.

Rationale behind Transfer Learning between 1D Molecule Sequences and 3D Conformers. The final goal of this transfer learning is to leverage the billion-scale 1D/2D molecule dataset to improve the 3D conformer prediction performance, which is constrained by limited 3D data. For clarity, we decompose the rationale into the following chain of arguments:

- **3D conformers are theoretically governed by 2D molecular graphs under quantum mechanics (QM).** 3D molecular properties and structures are fundamentally rooted in QM. Using (approximated) QM-based methods, like DFT, we can accurately predict 3D conformers from 2D molecular graphs, though at high computational cost. This establishes the critical role of 2D representations in determining 3D structures.
- **3D conformer prediction relies on high quality 2D molecule representations.** Deep learning models predict 3D conformers from 2D graphs, and their performance is heavily influenced by the quality of 2D molecular representations. Transfer learning can enhance 2D molecular representations, as demonstrated by prior works (Hu et al., 2020; Liu et al., 2022; Hou et al., 2022).
- **1D molecular representations can be converted to 2D molecular representations, and contribute to 3D prediction.** 1D molecule sequences encode the same information as 2D molecular graphs, and the 1D to 2D transformation can be achieved by deterministic toolkit, like RDkit. Leveraging RDkit and our proposed cross-modal projector (*cf.* Section 3.3), we can transform 1D molecular representations to 2D molecular representations, and therefore contribute to the 3D prediction. We have demonstrated this improvement in Table 4, where using the pretrained 1D representations improve 3D conformer prediction.
- **1D pretraining scales more effectively than 2D.** Given the billion-scale 1D/2D molecule dataset, we mostly prioritize the scalability when selecting the pretraining method. After literature review,

Table 15: Hyperparameters of the DMT-B and DMT-L models.

	DMT-B	DMT-L
n layers	10	12
atom hidden size	512	768
atom intermediate size	2048	3072
pair hidden size	128	192
pair intermediate size	512	768
n heads	8	8
total params	55M	150M
optimizer	AdamW	
init lr	1.00E-04	
min lr	1.00E-05	
warmup lr	1.00E-06	
warmup steps	1000	
weight decay	0.05	

we find that 1D LM-based pretraining methods, like Llama (Touvron et al., 2023) and BERT (Devlin et al., 2019), are extensively demonstrated for scalability and effectiveness. Therefore, we opt to 1D pretraining instead of 2D pretraining.

D Experimental Details

D.1 DMT Configurations

Hyperparameter. Table 15 shows the key hyperparameters used for training the DMT-B and DMT-L models. Other hyperparameters, like batch size and training epochs, are separately listed for each task in the following sections.

Features. We use the same atom features and pair features as (Jing et al., 2022). For the GEOM-DRUGS dataset, the atom feature has 74 dimensions; for the QM9-2014 and GEOM-QM9 datasets, the atom feature has 44 dimensions. The bond feature has 4 dimensions.

D.2 Task: *De Novo* Molecule Generation

For *De Novo* molecule generation, we separately train NEXT-Mol for the GEOM-DRUGS and the QM9-2014 datasets. This process involve training both the MoLlama and DMT of NExT-Mol.

MoLlama Settings. For QM9-2014, we use a batch size of 512 and train for 100 epochs, while for GEOM-DRUGS, we use a batch size of 256 and train for 20 epochs. For sampling, we employ a sampling temperature of 1.0 and, beam size of 1, and we sample 10,000 molecules for evaluation. We use the AdamW optimizer and a learning rate scheduler with linear warmup and cosine decay. The optimizer hyperparameters are as follows: init_lr=1e-4, min_lr=1e-5, warmup_lr=1e-6, warmup_steps=1000, and weight_decay=0.05.

DMT Settings. We use a dropout rate of 0.1 for QM9-2014 and 0.05 for GEOM-DRUGS. Following (Huang et al., 2024), we select only the conformer with the lowest energy for training on the GEOM-DRUGS dataset. For both datasets, we train DMT-B for 1000 epochs. The batch size for QM9-2014 is 2048 and the batch size for GEOM-DRUGS is 256.

Details on the Evaluation Metrics. We use the MMD distance when computing the distributional similarity of bond lengths, bond angles, and dihedral angles. Kekulization is performed when computing molecule and atom stability for 2D molecules, but not 3D molecules. We use canonicalized SMILES for both the generated molecules and the training dataset when computing novelty and uniqueness of molecules. All the baselines are consistently evaluated under the same setting above.

D.3 TASK: 3D CONFORMER PREDICTION

Training Details. We elaborate the training details for each of the three training stages in Section 3.3.

- **Stage 1: DMT Training.** For GEOM-QM9, we train the DMT-B model for 2000 epochs with a batch size of 2048. For GEOM-DRUGS, we train both the DMT-B and DMT-L models for 3000 epochs with batch size 256. Note that, for each epoch, we randomly sample a 3D conformer for each molecule, but not enumerate all the 3D conformers of that molecule. The resulting models (*i.e.,* DMT-B and DMT-L) are used directly for evaluation in Table 3.
- **Stage 2: Projector Warmup.** For both datasets, we train only the LoRA weights of MoLlama, and the cross-modal projector for 10 epochs. The pretrained weights of DMT and MoLlama are frozen throughout the process.
- **Stage 3: Integrated Fine-tuning.** For both datasets, we train the integrated model for 500 epochs. We train the LoRA weight of MoLlama, the cross-modal pojector, and the DMT model. The pretrained weights of MoLlama are frozen throughout the process.

Evaluation. Following (Wang et al., 2024; Jing et al., 2022), we use the dataset split of 243473/30433/1000 for GEOM-DRUGS and 106586/13323/1000 for GEOM-QM9, provided by (Ganea et al., 2021). For a molecule with K ground truth conformers, we generate $2K$ conformers as predictions.

Evaluation Metrics. Let $\{C_l^*\}_{l\in[1,L]}$ be the L predicted conformers and let $\{C_k\}_{k\in[1,K]}$ be the K ground truth conformers. The evaluation metrics AMR-R (AMR-Recall) and COV-R (COV-Recall) can be formally defined as follows:

$$\text{COV-R} := \frac{1}{L}|\{l \in [1..L] : \exists k \in [1..K], \text{RMSD}(C_k, C_l^*) < \delta\}|, \tag{14}$$

$$\text{AMR-R} := \frac{1}{L}\sum_{l\in[1..L]} \min_{k\in[1..K]} \text{RMSD}(C_k, C_l^*), \tag{15}$$

where δ is a threshold that is set to $0.75\mathring{A}$ for GEOM-DRUGS and set to $0.5\mathring{A}$ for GEOM-QM9, following (Wang et al., 2024; Jing et al., 2022). AMR-P (AMR-Precision) and COV-P (COV-Precision) can be similarly defined by swapping the ground truth conformers and predicted conformers.

D.4 TASK: CONDITIONAL MOLECULE GENERATION

Details for Adapting NExT-Mol for Conditional Generation. For conditional molecule generation on the QM9-2014 dataset, we modify the NEXT-Mol architecture to incorporate property-specific information into both the MoLlama language model and the DMT conformer prediction model. This approach allows us to generate molecules with desired properties in both 1D sequence and 3D structure spaces.

- **Condioning MoLlama.** We implement a condition MLP to encode property information into a soft prompt. This MLP consists of two linear layers with a GELU activation function in between. It transforms a single property value into a 4-token sequence embedding, each token having the same dimensionality as the model's hidden size. The resulting soft prompt is prepended to the input sequence embeddings of SELFIES before being fed into the language model. We adjust the attention mask accordingly to ensure the model attends to these conditional tokens.
- **Condioning DMT.** We use an MLP to process the property value, followed by a linear projection to match the time embedding dimension. This processed condition is then added to the time embedding, allowing the diffusion process to be guided by the desired property throughout the denoising steps.

MoLlama Setting. For conditional molecule generation, we train MoLlama with a batch size of 256 for 100 epochs on the QM9-2014 dataset. We use a sampling temperature of 1.0, beam size of 5, and we sample 10,000 molecules for evaluation of each desired property.

DMT Setting. For the DMT-B model, we train with a batch size of 512 for 1000 epochs on the QM9-2014 dataset. We employ a dropout rate of 0 with 100 sampling steps for evaluation.

The optimizer and learning rate schedule are consistent with the *de novo* generation task, using AdamW with a linear warmup followed by cosine decay. We train the conditional generation model for six different quantum properties using the same optimization strategy as in the *de novo* generation task. Each model is trained on 4 NVIDIA A100-80GB GPUs.